

NASA Technical Memorandum 4003

Low-Speed Wind-Tunnel  
Results for Symmetrical  
NASA LS(1)-0013 Airfoil

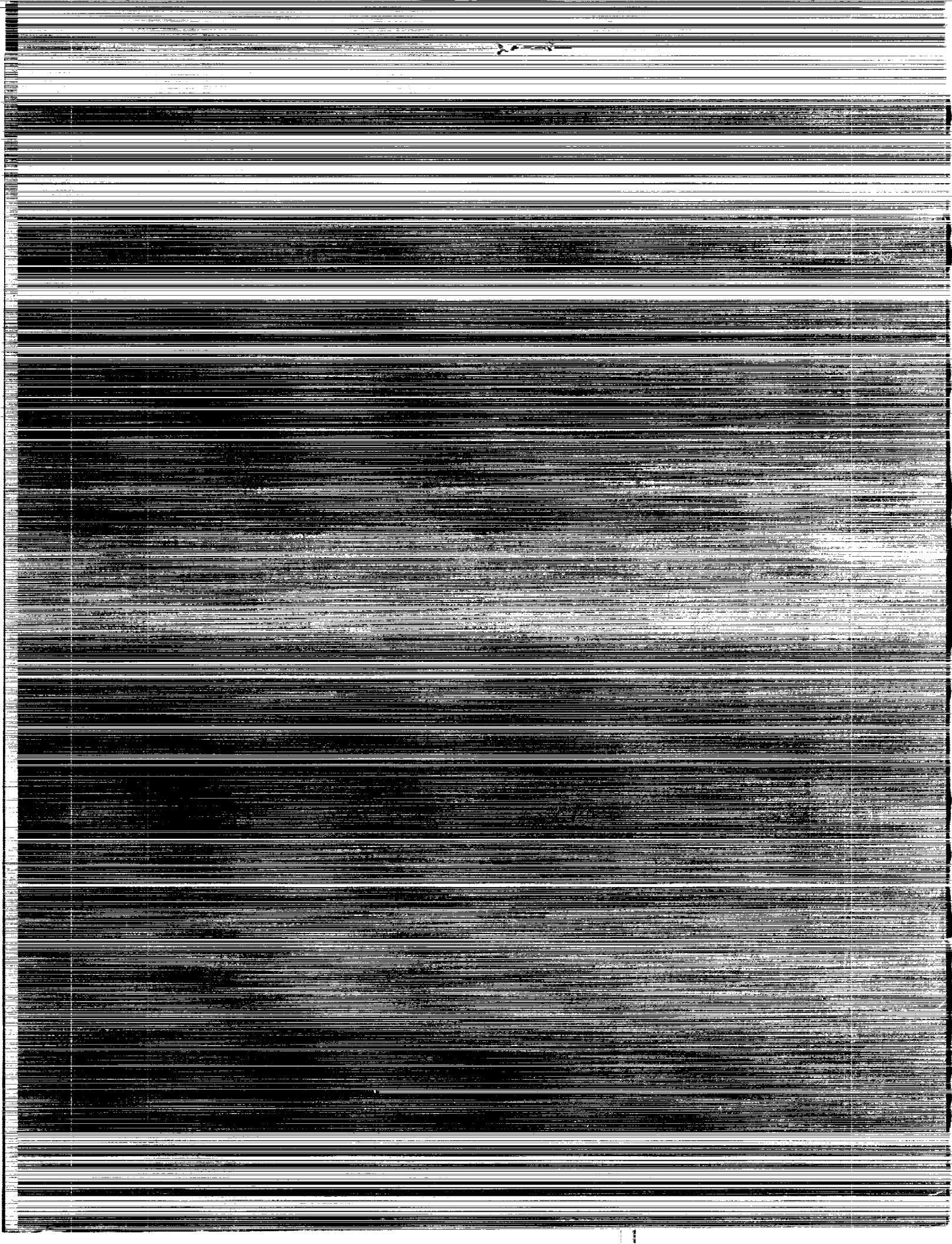
James C. Ferris, Robert J. McGhee,  
and Richard W. Barnwell

AUGUST 1987

(NASA-TM-4003) LOW-SPEED WIND-TUNNEL  
RESULTS FOR SYMMETRICAL NASA LS(1)-0013  
AIRFOIL (NASA) 38 p Avail: NTIS HC  
A03/MF A01

N87-26033

CSCL 01A      Unclas  
H1/02      0087898



NASA Technical Memorandum 4003

**Low-Speed Wind-Tunnel  
Results for Symmetrical  
NASA LS(1)-0013 Airfoil**

James C. Ferris, Robert J. McGhee,  
and Richard W. Barnwell

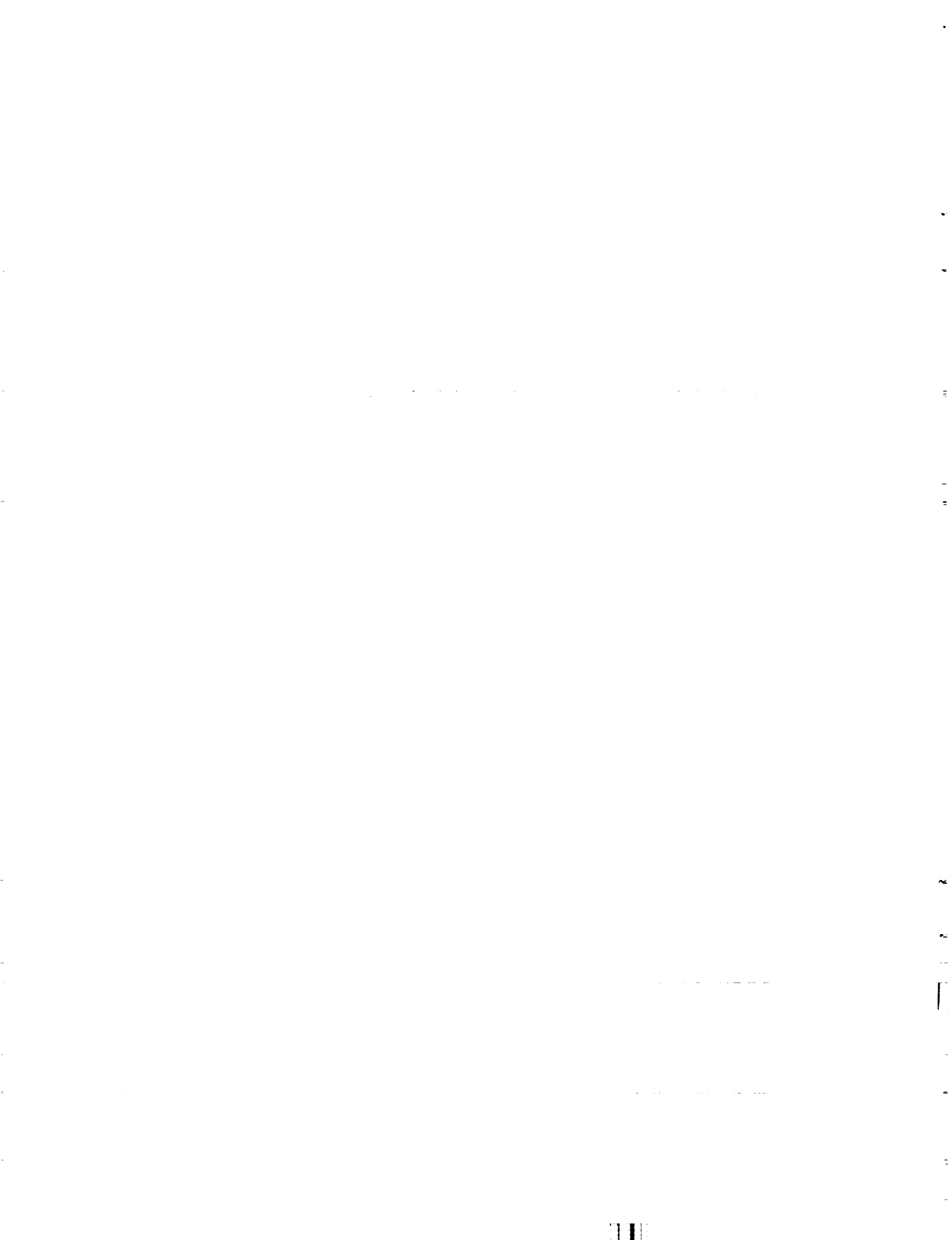
*Langley Research Center  
Hampton, Virginia*



National Aeronautics  
and Space Administration

**Scientific and Technical  
Information Office**

**1987**



## Summary

A wind-tunnel investigation was conducted in the Langley Low-Turbulence Pressure Tunnel to evaluate the performance of a symmetrical NASA LS(1)-0013 low-speed airfoil. The airfoil contour was obtained from the thickness distribution of a 13-percent-thick, high-performance airfoil developed for general aviation airplanes and is intended for use on the tail and other aerodynamic control surfaces. The tests were conducted at Mach numbers ( $M$ ) from 0.10 to 0.37 over a Reynolds number ( $R$ ) range from about  $0.6 \times 10^6$  to  $12.0 \times 10^6$ . The angle of attack varied from about  $-8^\circ$  to  $20^\circ$ .

The results indicate that the aerodynamic characteristics of the present airfoil are similar to those of the NACA 0012 airfoil. The lift-curve slope at small angles of attack for the present airfoil is slightly larger than that for the NACA 0012, and the maximum lift coefficient is also larger for Reynolds numbers greater than about  $4.0 \times 10^6$ . For smaller Reynolds numbers, the maximum lift coefficients for the two airfoils are about the same. The zero-lift drag coefficient with roughness applied is slightly greater for the present model for the test Reynolds numbers ( $2.2 \times 10^6$ ,  $4.0 \times 10^6$ , and  $6.0 \times 10^6$ ). The opposite trend was obtained for the airfoils without roughness. The stall characteristics of the present airfoil are of the turbulent or trailing-edge type. The stall angle of the present airfoil is  $1^\circ$  or  $2^\circ$  larger than that of the NACA 0012 airfoil. It is shown experimentally that about the same profile drag data are obtained with No. 80 and No. 90 grits for  $M = 0.15$  and  $R = 4 \times 10^6$  and essentially the same zero-lift drag coefficients are obtained for  $M = 0.15$  and  $R = 6 \times 10^6$  with No. 60, No. 80, No. 90, and No. 100 grits. The theoretical viscous analysis methods correctly predicted the lift, drag, and pitching-moment coefficients and chordwise pressure distributions for points at which the airfoil boundary layer is attached.

## Introduction

Research on advanced technology airfoils has received considerable attention at the Langley Research Center in the last several years. Reference 1 reports the results for an initial thickness family of airfoils developed for low-speed general aviation application. These results show that the 13-percent-thick member of this airfoil family provides the best overall performance (maximum lift and lift-drag ratio). In this report, the basic low-speed characteristics for a symmetrical version of this airfoil are presented. This symmetrical airfoil is intended for use on the tail and other aerodynamic control surfaces of general aviation airplanes.

The first series of low-speed airfoils is designated in the form NASA LS(1)-xxxx, where LS(1) indicates low speed (1st series), the next two digits give the design lift coefficient in tenths, and the last two digits indicate the maximum thickness in percent chord. Consequently, the present 13-percent-thick symmetric airfoil is designated the NASA LS(1)-0013 airfoil.

The investigation was performed in the Langley Low-Turbulence Pressure Tunnel at Mach numbers from 0.10 to 0.37. The chord Reynolds number varied from about  $0.6 \times 10^6$  to  $12.0 \times 10^6$ , and the geometric angle of attack varied from  $-8^\circ$  to  $20^\circ$ .

## Symbols

$C_p$	pressure coefficient, $\frac{p_L - p_\infty}{q_\infty}$
$c$	airfoil chord, in.
$c_c$	section chord-force coefficient, $\int C_p d\left(\frac{z}{c}\right)$
$c_d$	section profile-drag coefficient, $\int_{\text{Wake}} c'_d d\left(\frac{h}{c}\right)$
$c'_d$	point-drag coefficient (ref. 2)
$c_l$	section lift coefficient, $c_n \cos \alpha - c_c \sin \alpha$
$c_m$	section pitching-moment coefficient about quarter-chord point, $-\int C_p \left(\frac{x}{c} - 0.25\right) d\left(\frac{x}{c}\right) + \int C_p \frac{z}{c} d\left(\frac{z}{c}\right)$
$c_n$	section normal-force coefficient, $-\int C_p d\left(\frac{x}{c}\right)$
$h$	vertical distance in wake profile, in.
$M$	free-stream Mach number
$p$	static pressure, lb/ft <sup>2</sup>
$q$	dynamic pressure, lb/ft <sup>2</sup>
$R$	Reynolds number based on free-stream conditions and airfoil chord
$t$	airfoil thickness, in.
$x$	airfoil abscissa, in.
$z$	airfoil ordinate, in.
$z_t$	mean thickness, in.
$\alpha$	geometric angle of attack, deg

Subscripts:

L local point on airfoil

max	maximum
o	zero lift
$\infty$	undisturbed stream

## Model, Apparatus, and Procedure

### Model

The airfoil model consisted of a metal core with plastic fill to form the basic contour. (See table I.) Two thin layers of fiberglass were bonded to the plastic to form the smooth final surface. The contour of the airfoil is compared with that of the NACA 0012 airfoil in figure 1 and a comparison of the nondimensional thickness distributions of these airfoils is shown in figure 2. The model had a chord of 24 inches and a span of 36 inches. The model was equipped with both upper and lower surface orifices located 2 inches off the midspan. The airfoil surface was sanded in the chordwise direction with No. 400 dry silicon carbide paper to provide a smooth aerodynamic finish. The model contour accuracy was generally within  $\pm 0.004$  inch.

### Wind Tunnel

The Langley Low-Turbulence Pressure Tunnel (ref. 3) is a closed-throat, single-return tunnel which can be operated at stagnation pressures from 1 to 10 atmospheres with wind-tunnel empty-test-section Mach numbers up to 0.42 and 0.22, respectively. The maximum unit Reynolds number per foot is about  $15.0 \times 10^6$  at a Mach number of about 0.22. The tunnel test section is 3 feet wide by 7.5 feet high.

Hydraulically actuated circular plates provided positioning and attachment for the two-dimensional model. The plates are 40 inches in diameter, rotate with the airfoil, and are flush with the tunnel wall. The airfoil ends were attached to rectangular model attachment plates (fig. 3), and the airfoil was mounted so that the center of rotation of the circular plates was at  $0.25c$  on the model reference line. The air gaps at the tunnel walls between the rectangular plates and the circular plates were sealed with flexible sliding metal seals shown in figure 3. Tunnel sidewall boundary-layer control was not available for this test.

### Wake Survey Rake

A fixed wake survey rake (fig. 4) at the model midspan was cantilever mounted from the tunnel sidewall and located 1 chord behind the trailing edge

of the airfoil. The wake rake utilized total-pressure tubes, 0.060 inch in diameter, and static-pressure tubes, 0.125 inch in diameter. The total-pressure tubes were flattened to 0.040 inch for 0.24 inch from the tip of the tube. The static-pressure tubes each had four flush orifices drilled  $90^\circ$  apart, longitudinally located 8 tube diameters from the tip of the tube, and radially located in and perpendicular to the measurement plane of the total-pressure tubes.

### Instrumentation

Measurements of the static pressures on the airfoil surface and the wake rake pressures were made simultaneously by an automatic pressure-scanning system with variable-capacitance-type precision transducers. Basic tunnel pressures were measured with precision quartz manometers. Angle of attack was measured with a calibrated digital shaft encoder operated by a pinion gear and rack attached to the circular model attachment plates. Data were obtained by a high-speed acquisition system and recorded on magnetic tape.

### Test and Methods

The airfoil was tested at Mach numbers from 0.10 to 0.37 over an angle-of-attack range from about  $-8^\circ$  to  $20^\circ$ . Reynolds number based on the airfoil chord was varied from about  $0.6 \times 10^6$  to  $12.0 \times 10^6$ . The airfoil was tested both smooth (natural transition) and with roughness located on both upper and lower surfaces at  $0.075c$ . In general, the roughness was sized for each Reynolds number according to reference 4; however, a limited roughness study was conducted to verify the appropriate roughness sizes. The roughness consisted of granular-type strips 0.05 inch wide, sparsely distributed, and attached to the airfoil surface with clear lacquer.

The static-pressure measurements at the airfoil surface were reduced to standard pressure coefficients and machine integrated to obtain section normal-force and chord-force coefficients and section pitching-moment coefficients about the quarter-chord. The section profile-drag coefficient was computed from the wake-rake total and static pressures by the method reported in reference 2.

An estimate of the standard low-speed, wind-tunnel boundary corrections (ref. 5) amounted to a maximum of about 2 percent of the measured coefficients; therefore, these corrections have not been applied to the data.

## Presentation of Results

The results of this investigation have been reduced to coefficient form and are presented in the following figures:

Figure

Effect of Reynolds number on section characteristics for NASA LS(1)-0013 airfoil at $M \leq 0.15$ with model smooth . . . . .	5	Comparison of experimental and theoretical section characteristics for NASA LS(1)-0013 airfoil at $M = 0.15$ and $R = 6.0 \times 10^6$ with transition fixed at $0.075c$ . . . . .	15
Effect of Reynolds number on section characteristics for NASA LS(1)-0013 airfoil at $M \leq 0.15$ with transition fixed at $0.075c$ . . . . .	6	Comparison of section characteristics for NASA LS(1)-0013 and NACA 0012 airfoils at $M = 0.15$ with transition fixed at $0.075c$ . . . . .	16
Effect of roughness on section characteristics for NASA LS(1)-0013 airfoil at $M = 0.15$ . . . . .	7	Variation of maximum section lift coefficient with Reynolds number for NASA LS(1)-0013 and NACA 0012 airfoils at $M \leq 0.15$ . . . . .	17
Effect of roughness size on zero-lift drag coefficient for NASA LS(1)-0013 airfoil at $M = 0.15$ and $R = 6.0 \times 10^6$ . . . . .	8	Variation of maximum section lift coefficient with Mach number for NASA LS(1)-0013 and NACA 0012 airfoils at $R = 6.0 \times 10^6$ with transition fixed at $0.075c$ . . . . .	18
Effect of Mach number on section characteristics for NASA LS(1)-0013 airfoil at $R = 6.0 \times 10^6$ with transition fixed at $0.075c$ . . . . .	9	Variation of zero-lift drag coefficient with Reynolds number for NASA LS(1)-0013 and NACA 0012 airfoils at $M \leq 0.15$ . . . . .	19
Effect of angle of attack on pressure distribution for NASA LS(1)-0013 airfoil at $M = 0.15$ and $R = 2.2 \times 10^6$ with transition fixed at $0.075c$ . . . . .	10	Variation of zero-lift drag coefficient with Mach number for NASA LS(1)-0013 and NACA 0012 airfoils at $R = 6.0 \times 10^6$ with transition fixed at $0.075c$ . . . . .	20
Effect of angle of attack on pressure distribution for NASA LS(1)-0013 airfoil at $M = 0.15$ and $R = 4.0 \times 10^6$ with transition fixed at $0.075c$ . . . . .	11		
Effect of angle of attack on pressure distribution for NASA LS(1)-0013 airfoil at $M = 0.15$ and $R = 6.0 \times 10^6$ with transition fixed at $0.075c$ . . . . .	12		
Comparison of experimental and theoretical chordwise pressure distributions for NASA LS(1)-0013 airfoil at $M = 0.15$ and $R = 6.0 \times 10^6$ with transition fixed at $0.075c$ . . . . .	13		
Comparison of experimental and theoretical section characteristics for NASA LS(1)-0013 airfoil at $M = 0.15$ and $R = 4.0 \times 10^6$ with transition fixed at $0.075c$ . . . . .	14		

## Discussion of Results

### Experimental Results

**Airfoil smooth.** Figure 5 shows that with the airfoil smooth (natural boundary-layer transition), a lift-curve slope of about 0.12 per degree was obtained at small angles of attack for all test Reynolds numbers. Maximum lift coefficients increased from about 1.0 to about 1.8 as the Reynolds number was increased from about  $0.6 \times 10^6$  to  $9.0 \times 10^6$ , and the angle of attack at which the maximum lift coefficient occurred increased from about  $13^\circ$  to about  $19^\circ$  over this Reynolds number range. No appreciable change is noted in the maximum lift coefficient or the angle of attack at which maximum lift occurs when the Reynolds number is increased above  $9.0 \times 10^6$ . The stall characteristics of the airfoil are of the turbulent or trailing-edge type as shown by the lift data of figure 5 and the pressure data of figures 10, 11, and 12.

The pitching-moment coefficient data with the airfoil smooth (fig. 5) are generally insensitive to Reynolds numbers from about  $2.0 \times 10^6$  to  $12.0 \times 10^6$ . A decrease in Reynolds number below about  $2.0 \times 10^6$  causes a positive increment in  $c_m$  for angles of attack greater than about  $9^\circ$ .

The profile-drag data of figures 5 and 19 show a reduction in the drag coefficient in the low drag range up to a Reynolds number of about  $4 \times 10^6$ . The increase in drag at the higher Reynolds numbers is a result of the decrease in the extent of laminar flow on the model. The minimum drag coefficient measured was about 0.0056.

**Roughness effect.** The addition of roughness at 0.075c (figs. 6 and 7) had no appreciable effect on the lift curves for this airfoil for Reynolds numbers of  $2.2 \times 10^6$ ,  $4.0 \times 10^6$ , and  $6.0 \times 10^6$  at  $M = 0.15$ . The maximum lift coefficient was unaffected by the addition of roughness under these conditions. (See fig. 17.) The addition of roughness causes no appreciable change in the pitching-moment coefficient for  $M = 0.15$  and Reynolds numbers of  $2.2 \times 10^6$ ,  $4.0 \times 10^6$ , and  $6.0 \times 10^6$ . The addition of roughness forces transition to turbulent flow at the chord station of 0.075c and thus increases the drag coefficient. This effect is particularly large in the range of lift coefficient between  $-0.3$  and  $0.3$  where the extent of laminar flow on the smooth model can be appreciable.

An attempt has been made to determine to what extent the drag data is affected by roughness size. Figure 7(b) shows that about the same profile-drag data are obtained with No. 80 and No. 90 grits for  $M = 0.15$  and  $R = 4.0 \times 10^6$ . It can be seen in figure 8 that essentially the same zero-lift drag coefficients are obtained for  $M = 0.15$  and  $R = 6.0 \times 10^6$  with No. 60, No. 80, No. 90, and No. 100 grits. For most general aviation applications, the drag data of most practical interest are thought to be those obtained with roughness applied since transition is usually fixed near the leading edge by construction roughness or insect remains gathered in flight. However, new structural materials and fabrication techniques would enable the use of laminar-flow airfoils on general aviation airplanes.

**Mach number effects.** Figure 9 shows that at a Reynolds number of  $6.0 \times 10^6$  with transition fixed at 0.075c, the lift characteristics do not vary appreciably for Mach numbers below 0.20. The maximum lift coefficient and the angle of attack at which it occurs vary smoothly with Mach numbers from 0.20 to 0.37. This same Mach number increase results in a decrease of about  $6^\circ$  in the angle of attack for stall and a decrease in  $c_{l,\max}$  of about 0.50. For a Reynolds number of  $6.0 \times 10^6$  with transition fixed at 0.075c (fig. 9), the pitching-moment coefficient is insensitive to Mach number change from 0.10 to 0.20. An increase in the Mach numbers above 0.20 causes a

positive increment in  $c_m$  for angles of attack greater than about  $8^\circ$ .

Figure 9 shows that the profile-drag data for  $R = 6.0 \times 10^6$  with transition fixed at 0.075c are not affected appreciably by Mach numbers from 0.10 to 0.37 for lift coefficients between about  $-1$  and  $1$ . For larger lift coefficients, the general effect of increasing Mach number is to increase the drag coefficient.

**Pressure distributions.** The chordwise pressure data of figures 10, 11, and 12 illustrate the effects of angle of attack for  $M = 0.15$  and Reynolds numbers of  $2.2 \times 10^6$ ,  $4.0 \times 10^6$ , and  $6.0 \times 10^6$ , respectively, with transition fixed at 0.075c. The symmetry of the model is indicated by the coincidence of the upper and lower surface data for  $\alpha = 0^\circ$  and the coincidence of the data from opposite surfaces of the airfoil for  $\alpha = 4.0^\circ$  and  $-4.0^\circ$ . The airfoil stall is of the turbulent or trailing-edge type and is reflected somewhat in the pressure distributions at the highest angles of attack.

Experimental and theoretical data predictions of the chordwise pressure distributions by the methods of references 6 and 7 are compared with the experimental data at  $M = 0.15$  and  $R = 6.0 \times 10^6$  for angles of attack of  $4^\circ$  and  $8^\circ$  in figure 13. Both methods predict the pressure distribution well; however, there are some slight differences over the aft 20-percent chord.

Predictions of the aerodynamic characteristics by the viscous method of reference 6 are compared at a Mach number of 0.15 and Reynolds number of  $4.0 \times 10^6$  in figure 14 with experimental results for angles of attack at which the flow is attached. The Reynolds number is increased to  $6.0 \times 10^6$  in the data in figure 15, and predictions from reference 7 are also included. The theoretical methods predict the lift, drag, and pitching-moment data well over the range of angle of attack to  $12^\circ$ . The method of reference 7 predicts the drag coefficient somewhat low in the angle-of-attack range from  $8^\circ$  to  $12^\circ$ .

## Comparison of NASA LS(1)-0013 With NACA 0012 Airfoil

The section characteristics of the NASA LS(1)-0013 and the NACA 0012 airfoils at  $M = 0.15$  with transition fixed at 0.075c are compared in figure 16 for the Reynolds numbers  $2.0 \times 10^6$ ,  $4.0 \times 10^6$ , and  $6.0 \times 10^6$ . Both airfoils were tested in the Langley Low-Turbulence Pressure Tunnel. The lift-curve slope at small angles of attack for the NASA LS(1)-0013 is slightly larger, and the stall angle of attack for this airfoil is approximately  $1^\circ$  larger for Reynolds numbers of  $2.0 \times 10^6$  and  $4.0 \times 10^6$  and approximately  $2^\circ$  larger for the Reynolds number  $6.0 \times 10^6$ .

The maximum lift coefficients for the two airfoils (fig. 17) are approximately the same for Reynolds numbers of about  $4.0 \times 10^6$  and less. For larger Reynolds numbers, the maximum lift coefficient of the NASA LS(1)-0013 airfoil is larger. For example, for  $M = 0.15$  and  $R = 6.0 \times 10^6$  with transition fixed at  $0.075c$ , the values of  $C_{l,\max}$  for the NASA LS(1)-0013 and the NACA 0012 airfoils are about 1.75 and 1.65, respectively. The difference in  $C_{l,\max}$  diminishes with increasing Mach number (fig. 18). Figure 16 also shows that the pitching-moment coefficient for the NASA LS(1)-0013 airfoil is less than that for the NACA 0012 airfoil for all positive lift coefficients. In this range, the pitching-moment coefficient for the NASA LS(1)-0013 is zero or slightly negative, whereas that for the NACA 0012 is zero or slightly positive.

The section drag characteristics for the NASA LS(1)-0013 and the NACA 0012 airfoils at  $M = 0.15$  with transition fixed at  $0.075c$  (fig. 16) are about the same for Reynolds numbers of  $2.0 \times 10^6$ ,  $4.0 \times 10^6$ , and  $6.0 \times 10^6$ . Figure 19 shows that the drag coefficient at zero lift for the NASA LS(1)-0013 airfoil at  $M = 0.15$  with roughness applied is slightly greater than that for the NACA 0012 airfoil under similar conditions. The additional thickness of the LS(1)-0013 airfoil should cause the drag coefficient to be slightly higher. The opposite trend applies for the airfoils without roughness. This is a result of more laminar flow present on the LS(1)-0013 airfoil compared with that on the NACA 0012 airfoil. The zero-lift drag coefficients of both airfoils with roughness applied are independent of Mach number over the test range (fig. 20).

## Concluding Remarks

A wind-tunnel test has been conducted in the Langley Low-Turbulence Pressure Tunnel to evaluate the performance of a symmetrical NASA LS(1)-0013 airfoil. The contour of this symmetrical airfoil was obtained from the thickness distribution of a 13-percent-thick, high-performance airfoil developed for general aviation airplanes. The tests were conducted at Mach numbers ( $M$ ) from 0.10 to 0.37 over a Reynolds number ( $R$ ) range from about  $0.6 \times 10^6$  to  $12.0 \times 10^6$ . The angle of attack varied from about  $-8^\circ$  to  $20^\circ$ .

The results indicate that the aerodynamic characteristics of the present airfoil are similar to those of the NACA 0012 airfoil. The lift-curve slope for small angles of attack for the present airfoil is slightly larger; and the maximum lift coefficient for the present airfoil is larger for Reynolds numbers greater than about  $4.0 \times 10^6$ . For smaller Reynolds numbers, the maximum lift coefficients for the two

airfoils are about the same. The zero-lift drag coefficient with roughness applied is slightly greater for the present model for the test Reynolds numbers ( $2.2 \times 10^6$ ,  $4.0 \times 10^6$ , and  $6.0 \times 10^6$ ). This trend is consistent with the fact that the present airfoil is slightly thicker than the NACA 0012 airfoil. The opposite trend was obtained for the airfoils without roughness. This is a result of more laminar flow present on the LS(1)-0013 airfoil compared with that on the NACA 0012 airfoil. The stall characteristics of both airfoils are of the turbulent or trailing-edge type. The stall angle of the present airfoil is about  $1^\circ$  greater than that of the NACA 0012 airfoil for  $R = 2.2 \times 10^6$  and  $4.0 \times 10^6$  and about  $2^\circ$  greater for  $R = 6.0 \times 10^6$ . It was shown experimentally that about the same profile-drag data are obtained with No. 80 and No. 90 grit for  $M = 0.15$  and  $R = 4 \times 10^6$  and essentially the same zero-lift drag coefficients are obtained for  $M = 0.15$  and  $R = 6 \times 10^6$  with No. 60, No. 80, No. 90, and No. 100 grits. The theoretical viscous analysis methods correctly predicted the lift, drag, and pitching-moment coefficients and chordwise pressure distribution when the airfoil boundary layer is attached.

NASA Langley Research Center  
Hampton, VA 23665-5225  
June 24, 1987

## References

1. McGhee, Robert J.; and Beasley, William D.: *Effects of Thickness on the Aerodynamic Characteristics of an Initial Low-Speed Family of Airfoils for General Aviation Applications*. NASA TM X-72843, 1976.
2. Pankhurst, R. C.; and Holder, D. W.: *Wind-Tunnel Technique*. Sir Isaac Pitman & Sons, Ltd. (London), 1965.
3. McGhee, Robert J.; Beasley, William D.; and Foster, Jean M.: *Recent Modifications and Calibration of the Langley Low-Turbulence Pressure Tunnel*. NASA TP-2328, 1984.
4. Braslow, Albert L.; and Knox, Eugene C.: *Simplified Method for Determination of Critical Height of Distributed Roughness Particles for Boundary-Layer Transition at Mach Numbers From 0 to 5*. NACA TN 4363, 1958.
5. Pope, Alan; and Harper, John J.: *Low-Speed Wind Tunnel Testing*. John Wiley & Sons, Inc., 1966.
6. Smetana, Frederick O.; Summey, Delbert C.; Smith, Neill S.; and Carden, Ronald K.: *Light Aircraft Lift, Drag, and Moment Predictions—A Review and Analysis*. NASA CR-2523, 1975.
7. Bauer, Frances; Garabedian, Paul; Korn, David; and Jameson, Antony: *Supercritical Wing Sections II*. Volume 108 of *Lecture Notes in Economics and Mathematical Systems*, M. Beckmann and H. P. Kuenzi, eds., Springer-Verlag, 1975.

Table I. Measured Coordinates for NASA LS(1)-0013 Airfoil

Upper surface		Lower surface	
$x/c$	$z/c$	$x/c$	$z/c$
0.00000	0.00000	0.00000	0.00000
.00624	.01344	.00708	-.01435
.01255	.01892	.01301	-.01938
.01771	.02222	.01843	-.02283
.02470	.02583	.02505	-.02612
.03737	.03075	.03729	-.03080
.04998	.03465	.04993	-.03462
.06260	.03790	.06245	-.03788
.07535	.04075	.07498	-.04070
.10014	.04541	.10003	-.04543
.15007	.05245	.14914	-.05241
.19992	.05750	.19979	-.05755
.25029	.06094	.24982	-.06102
.30055	.06307	.29964	-.06316
.34984	.06407	.34958	-.06428
.40004	.06432	.39969	-.06453
.45013	.06374	.44988	-.06388
.50025	.06203	.50082	-.06209
.55021	.05896	.54984	-.05905
.60038	.05446	.59961	-.05459
.65028	.04868	.64938	-.04885
.70010	.04183	.69962	-.04196
.75018	.03429	.74964	-.03441
.80021	.02638	.79934	-.02654
.85035	.01859	.84858	-.01891
.90019	.01172	.90080	-.01165
.95029	.00633	.94991	-.00618
.98960	.00371	.99007	-.00358
1.00000	.00302	1.00000	-.00302

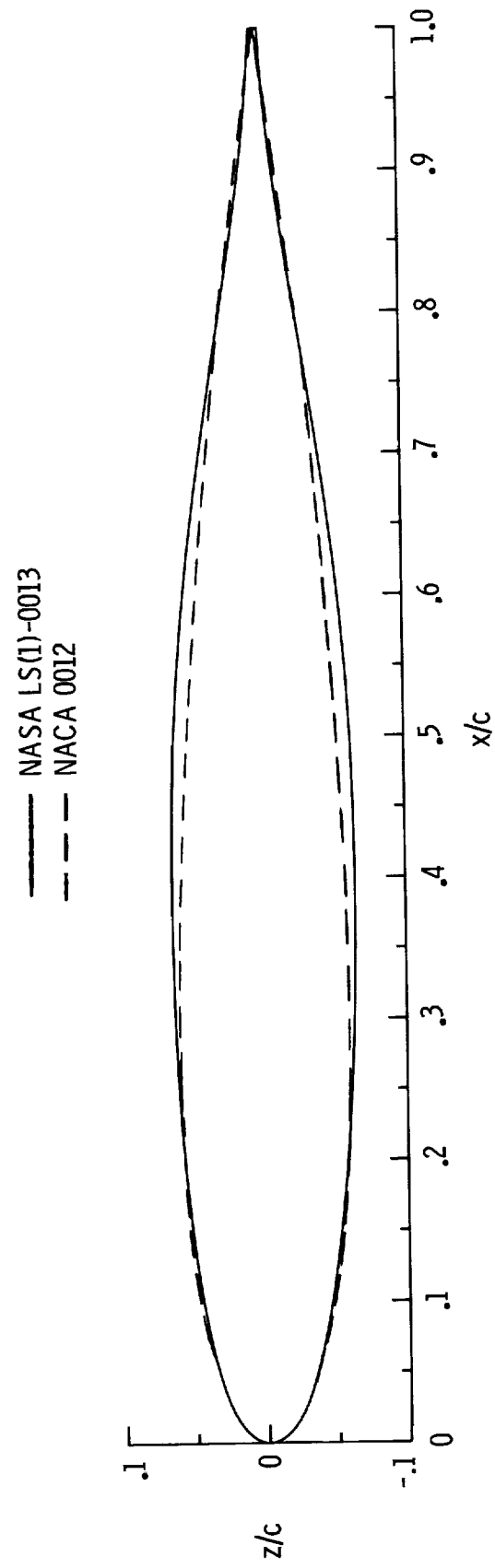


Figure 1. Profiles of NASA LS(1)-0013 and NACA 0012 airfoils.

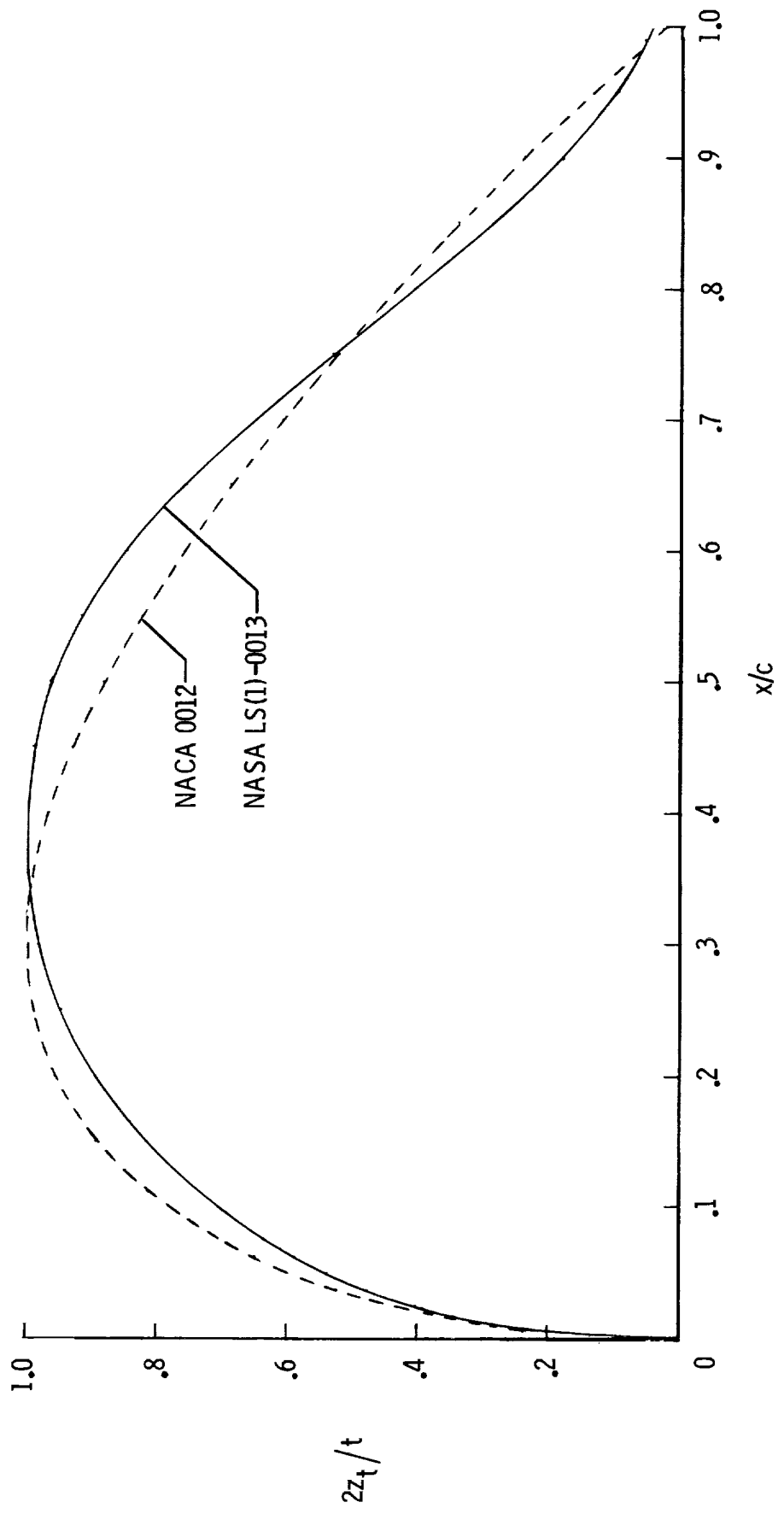


Figure 2. Comparison of nondimensional thickness distributions of NASA LS(1)-0013 and NACA 0012 airfoils.

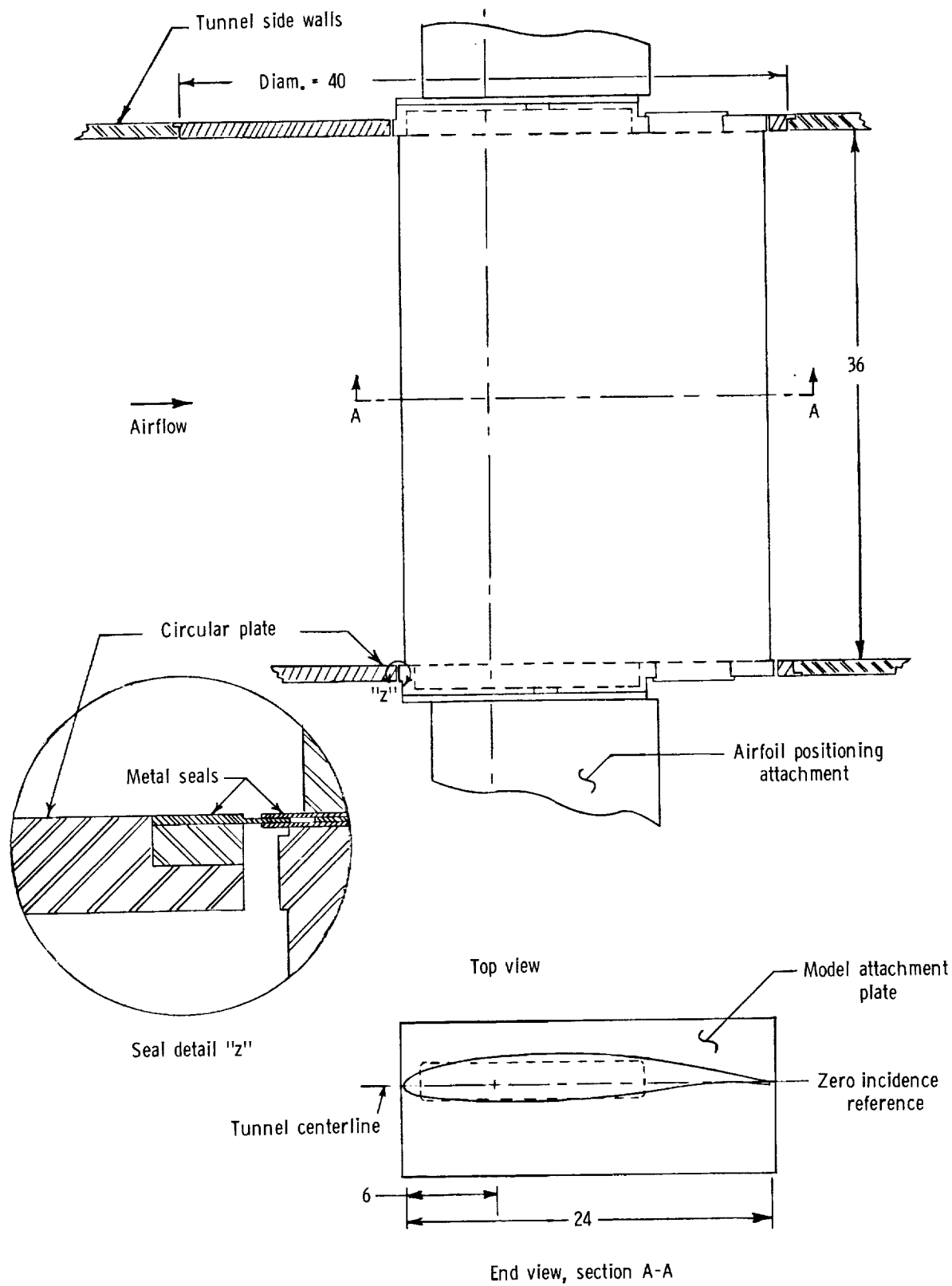


Figure 3. Typical airfoil mounted in wind tunnel. All dimensions are in inches.

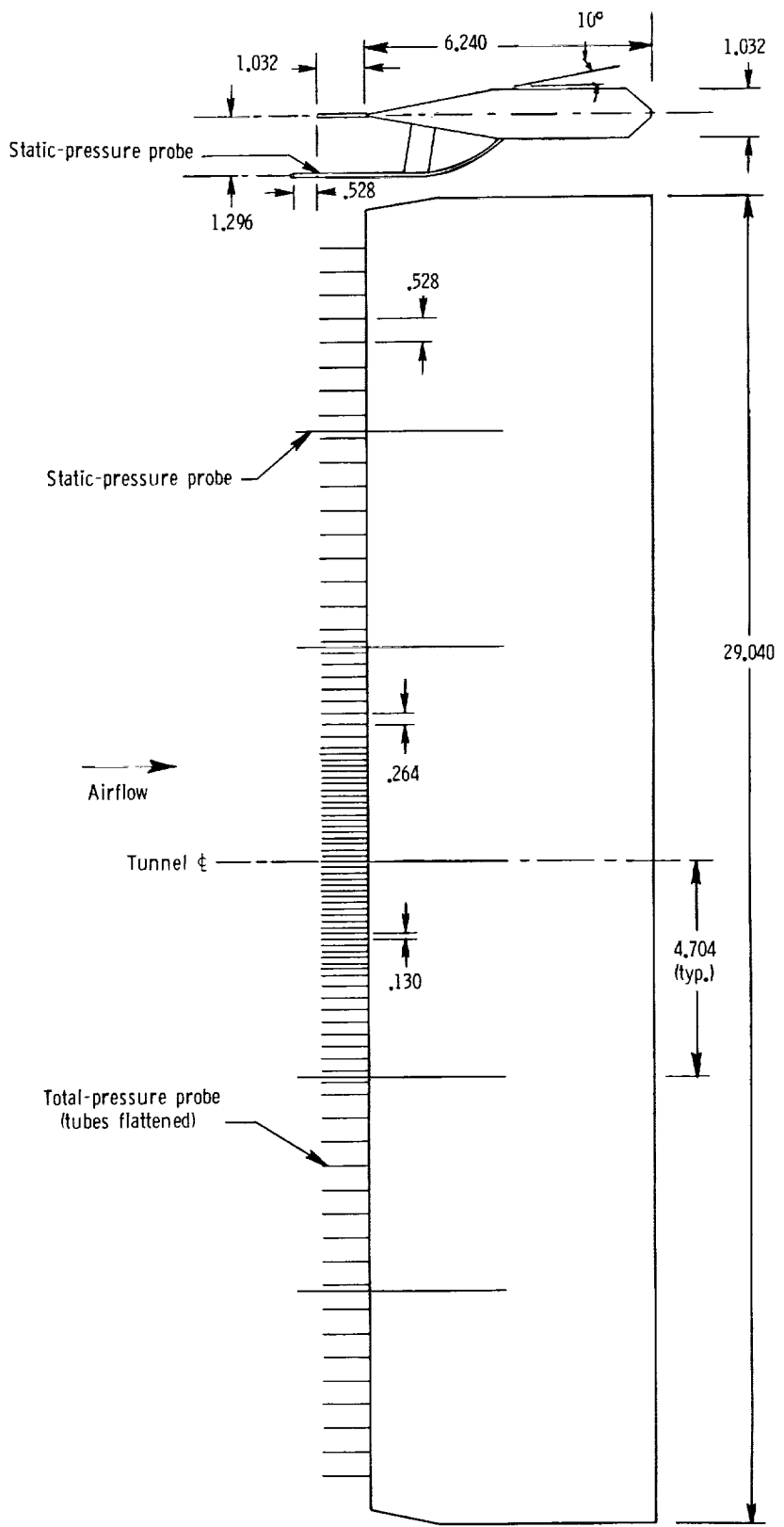
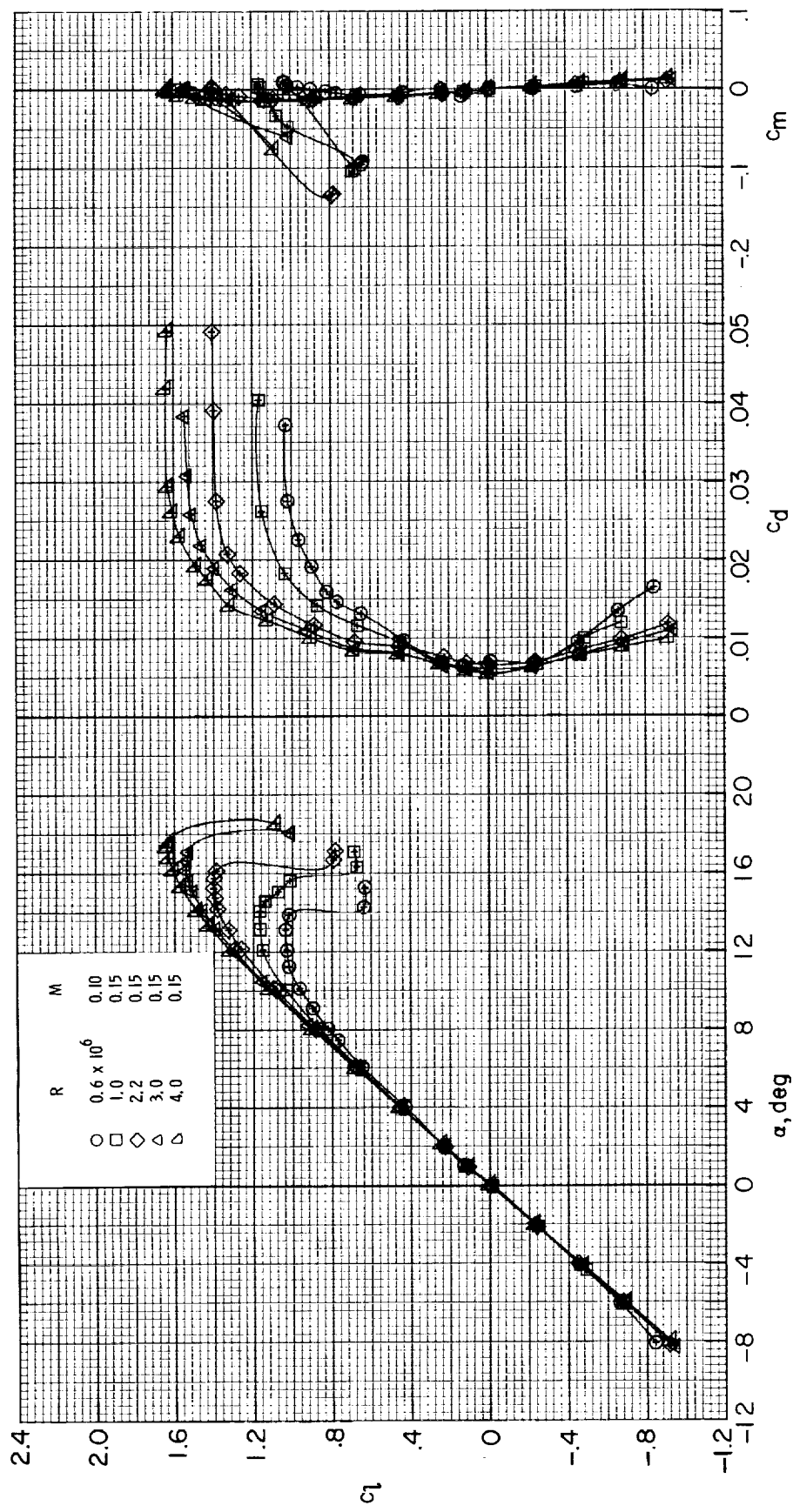
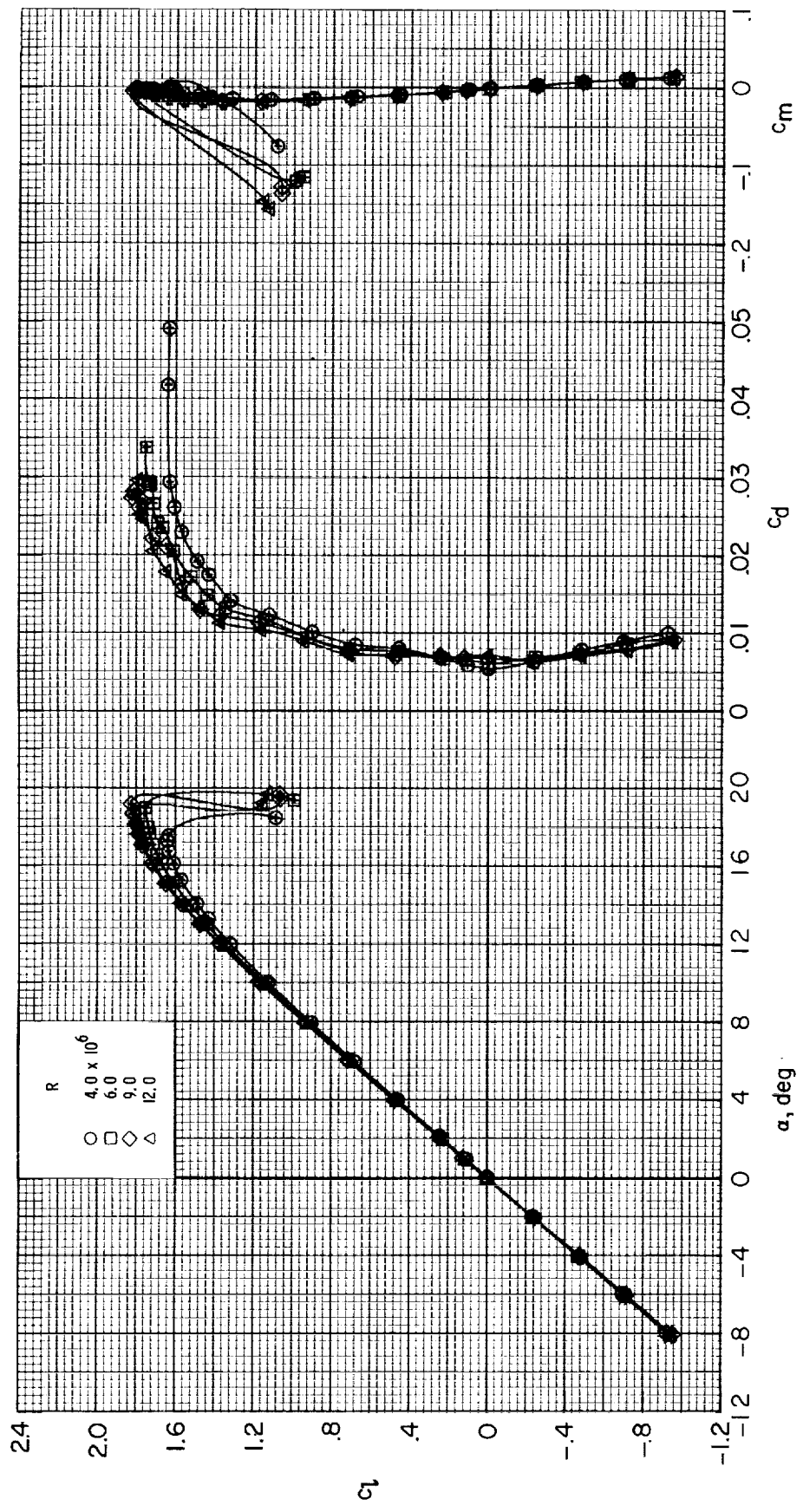


Figure 4. Drawing of wake survey rake. All dimensions are in inches.



(a)  $R \leq 4.0 \times 10^6$ .

Figure 5. Effect of Reynolds number on section characteristics for NASA LS(1)-0013 airfoil at  $M \leq 0.15$  with model smooth.



(b)  $R \geq 4.0 \times 10^6$ .

Figure 5. Concluded.

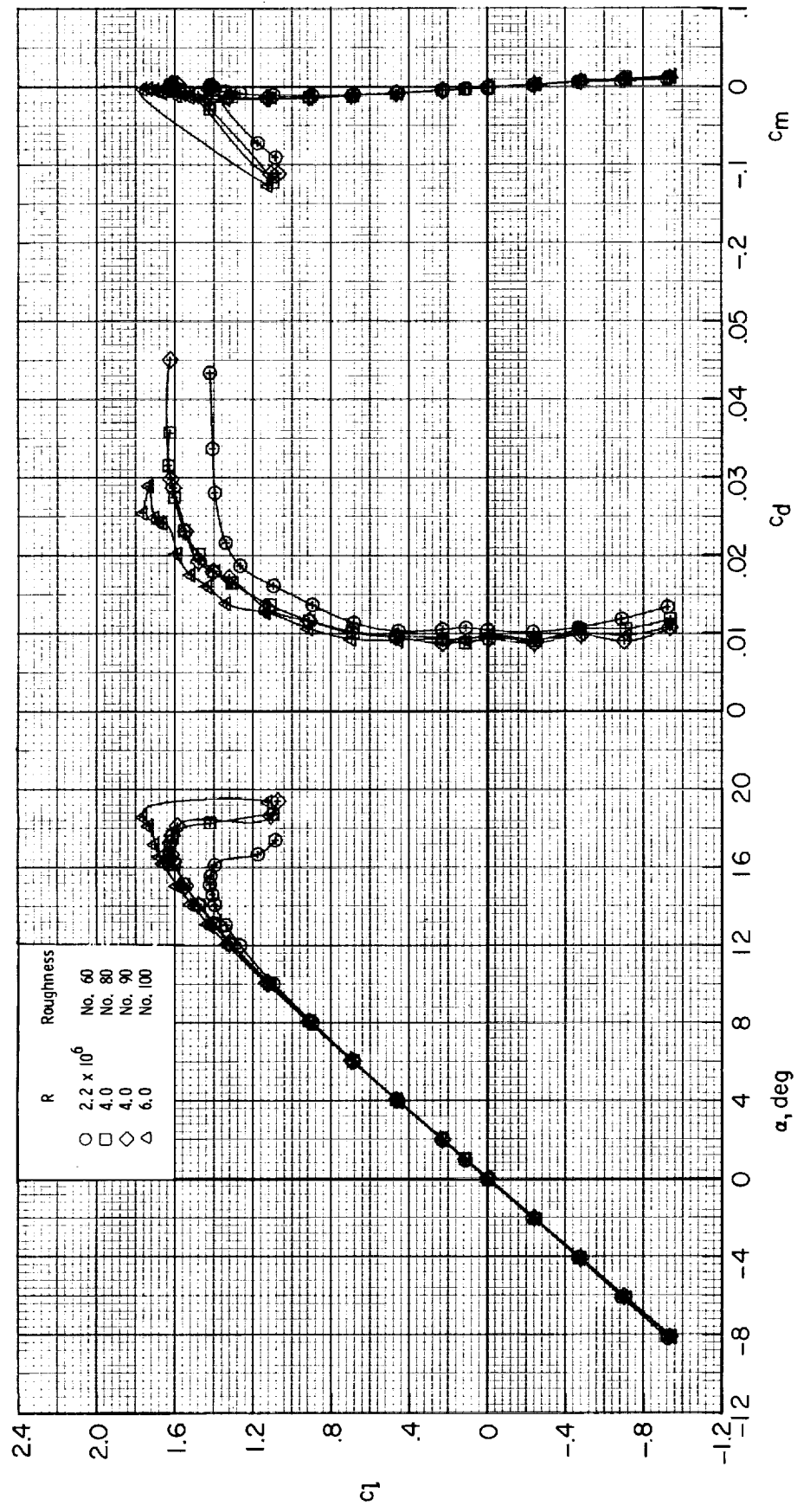
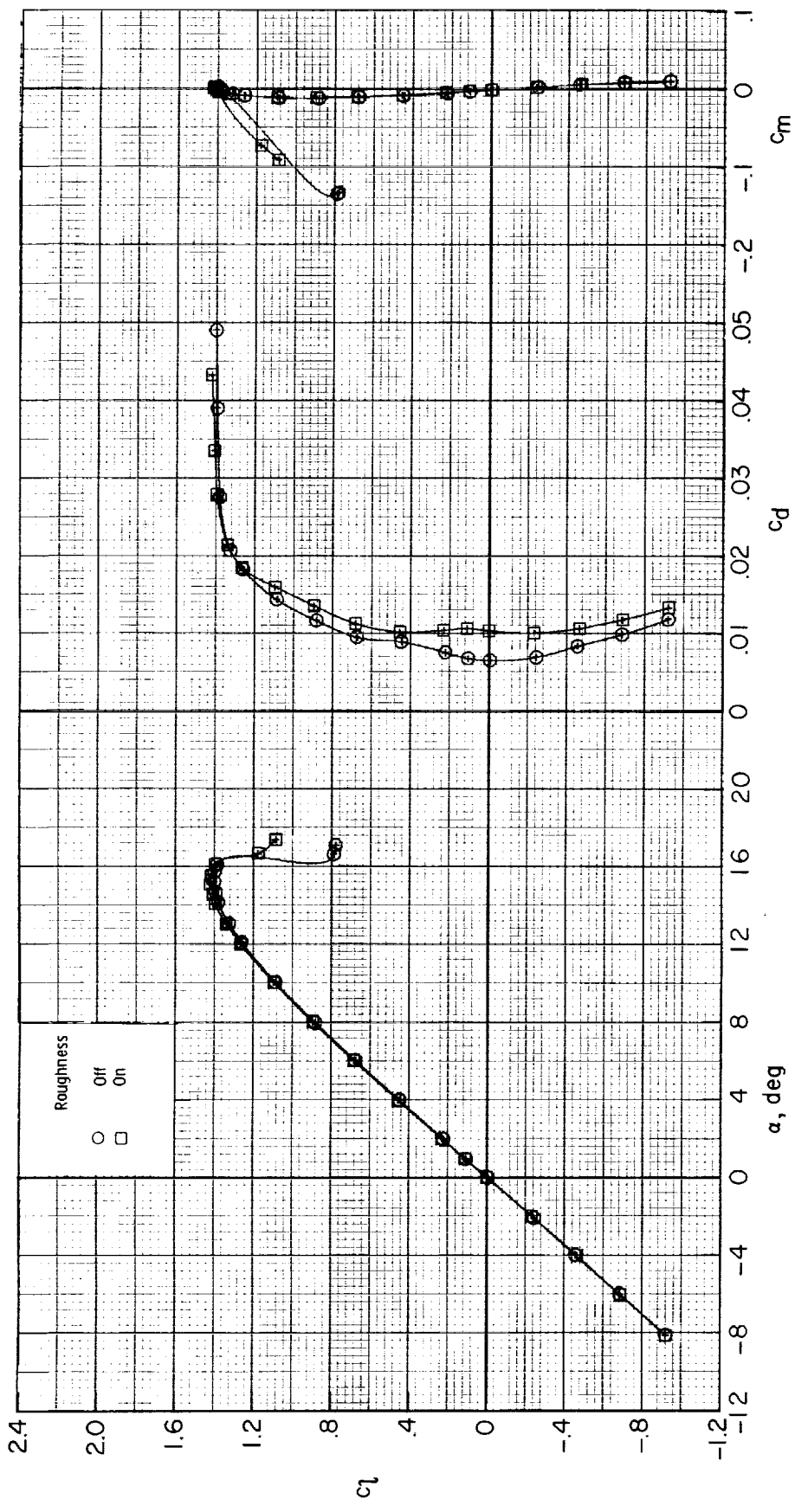
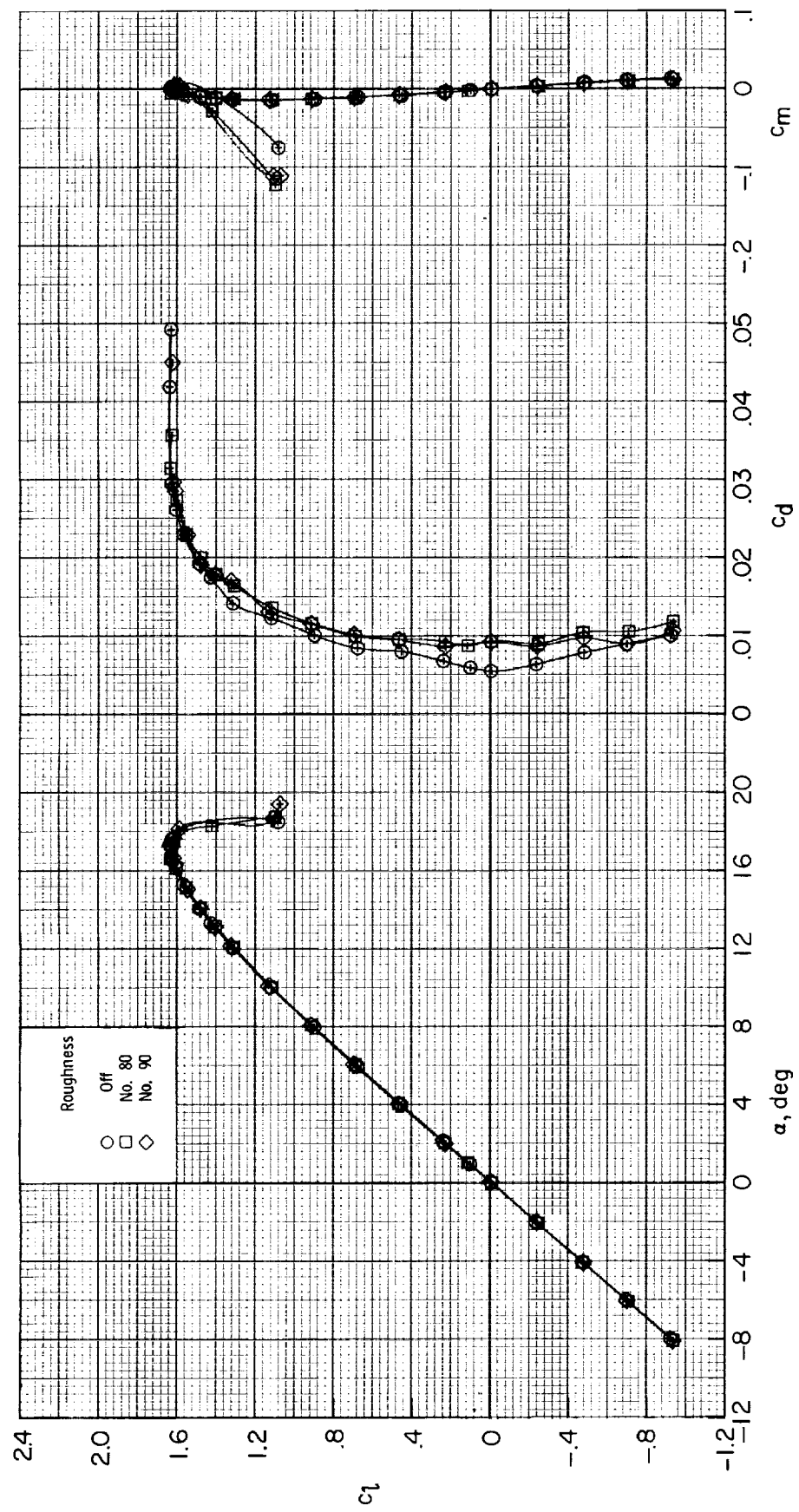


Figure 6. Effect of Reynolds number on section characteristics for NASA LS(1)-0013 airfoil at  $M \leq 0.15$  with transition fixed at 0.075c.



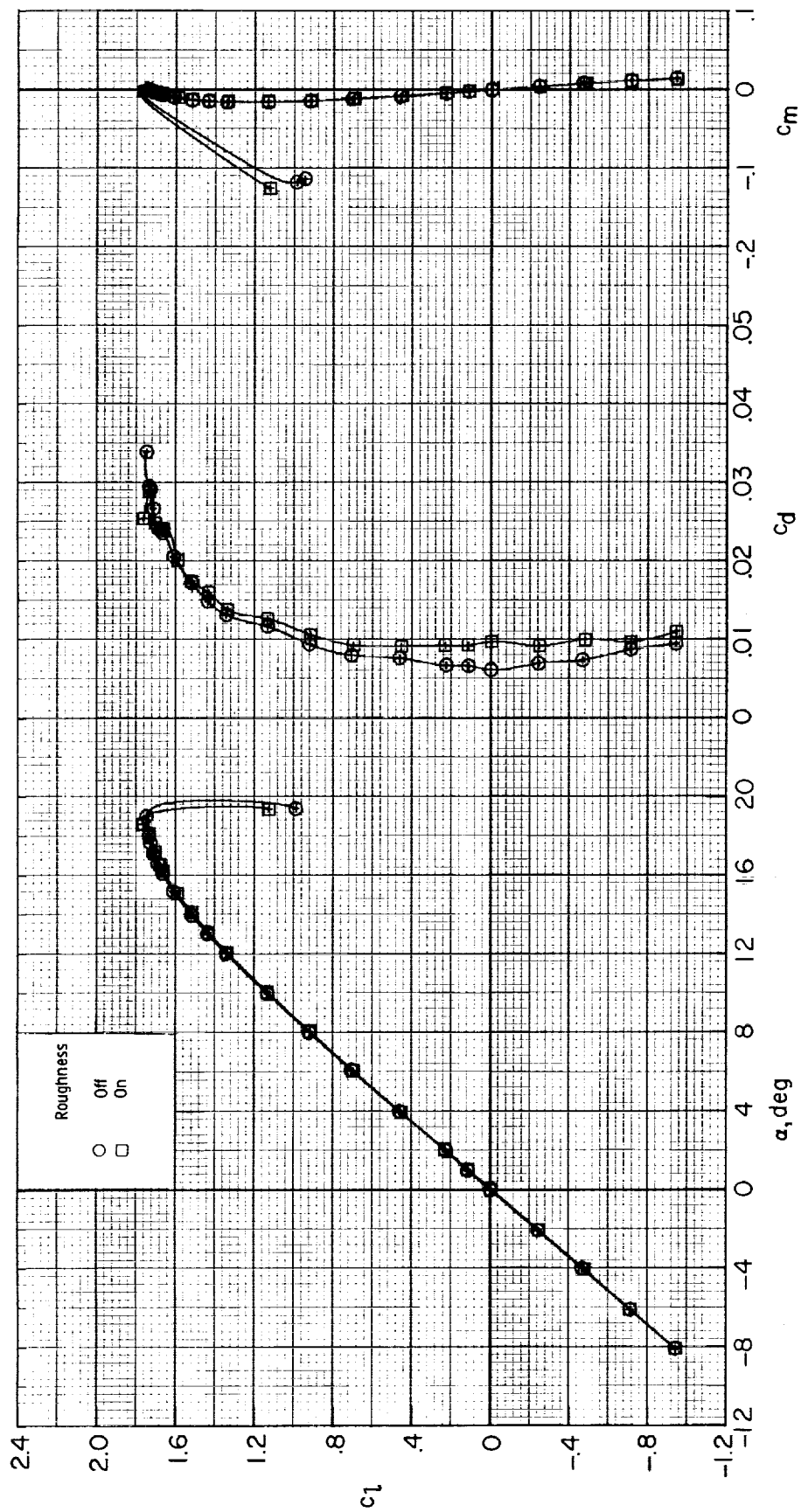
(a)  $R = 2.2 \times 10^6$ .

Figure 7. Effect of roughness on section characteristics for NASA LS(1)-0013 airfoil at  $M = 0.15$ .



(b)  $R = 4.0 \times 10^6$ .

Figure 7. Continued.



(c)  $R = 6.0 \times 10^6$ .

Figure 7. Concluded.

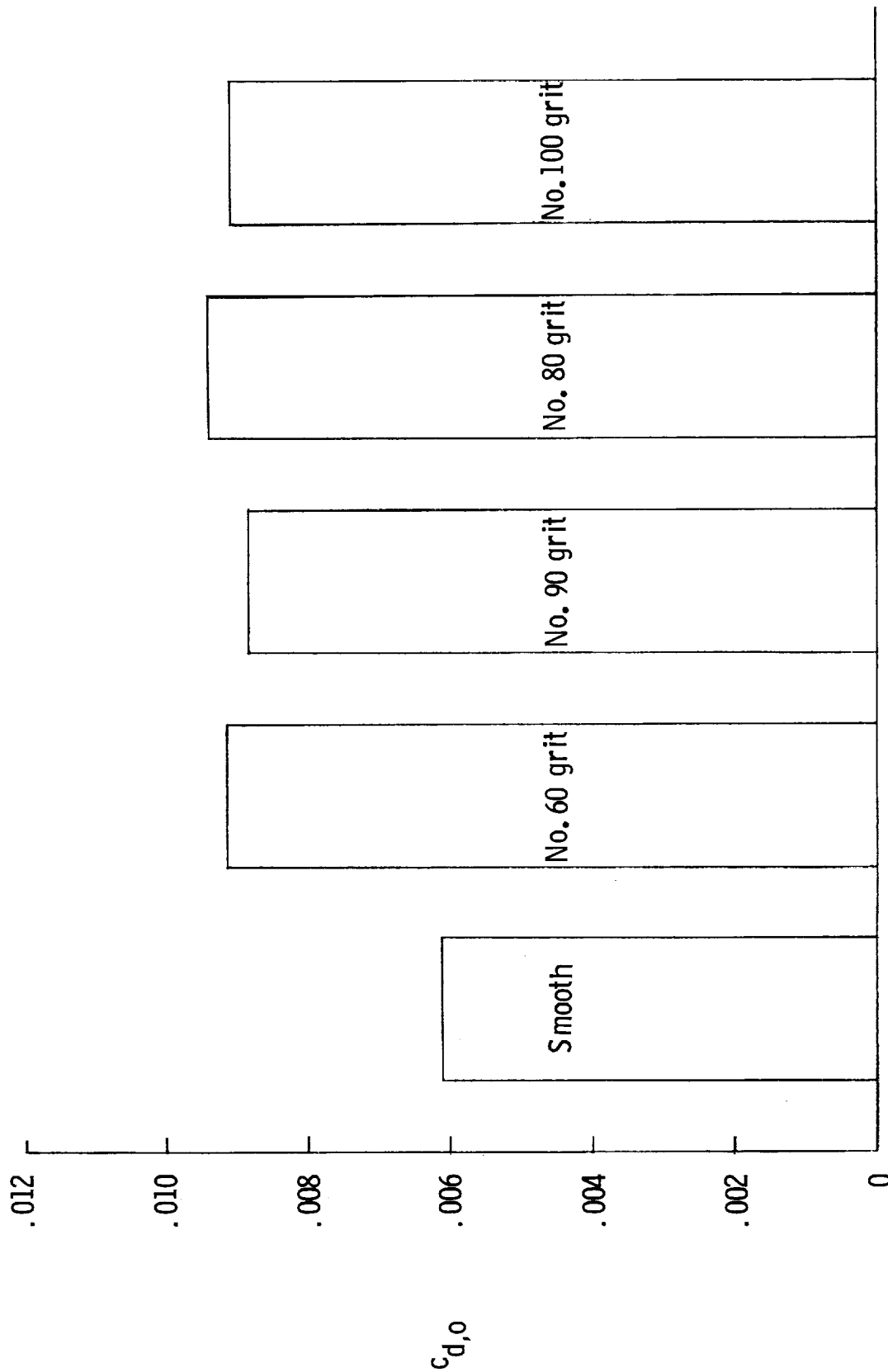


Figure 8. Effect of roughness size on zero-lift drag coefficient for NASA LS(1)-0013 airfoil at  $M = 0.15$  and  $R = 6.0 \times 10^6$ .

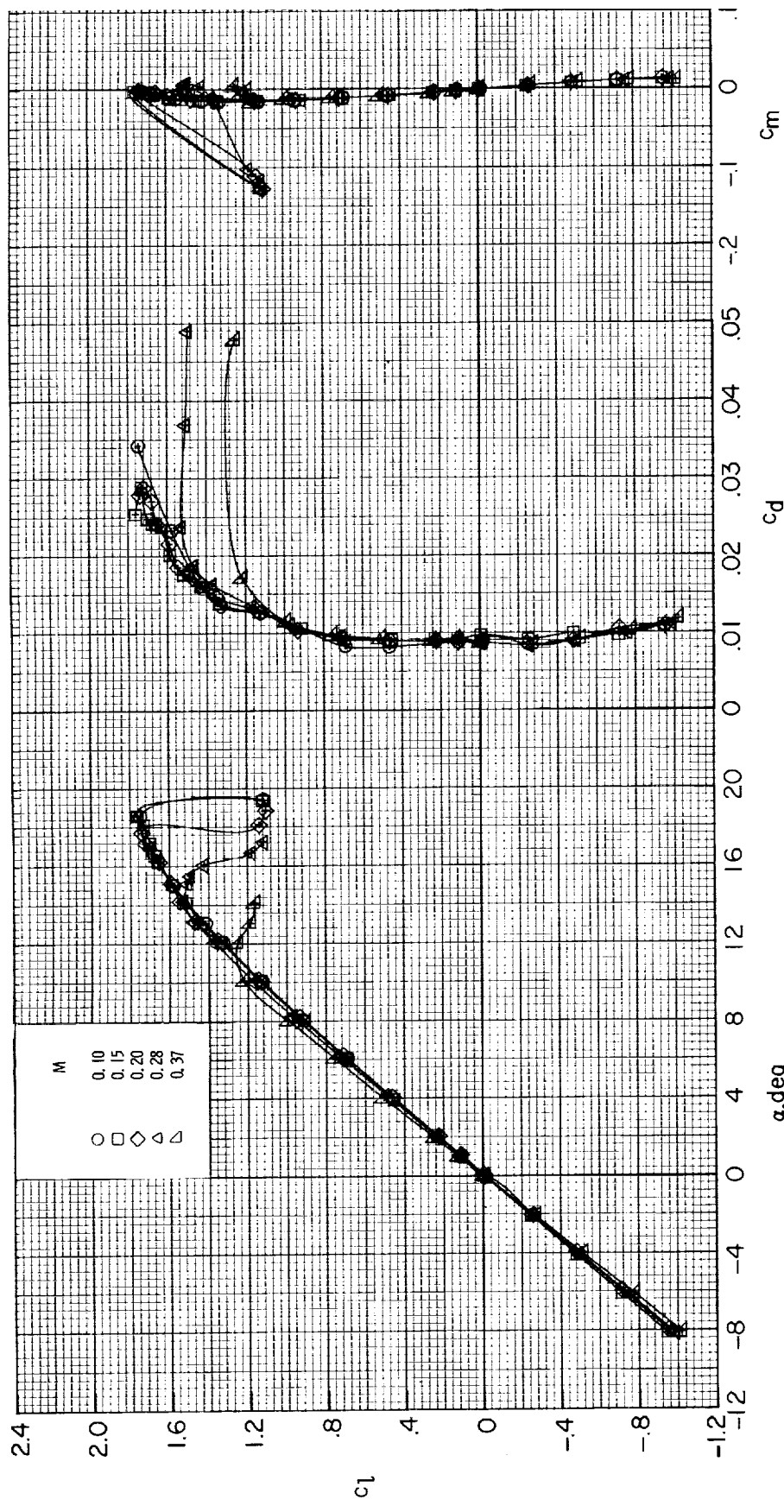
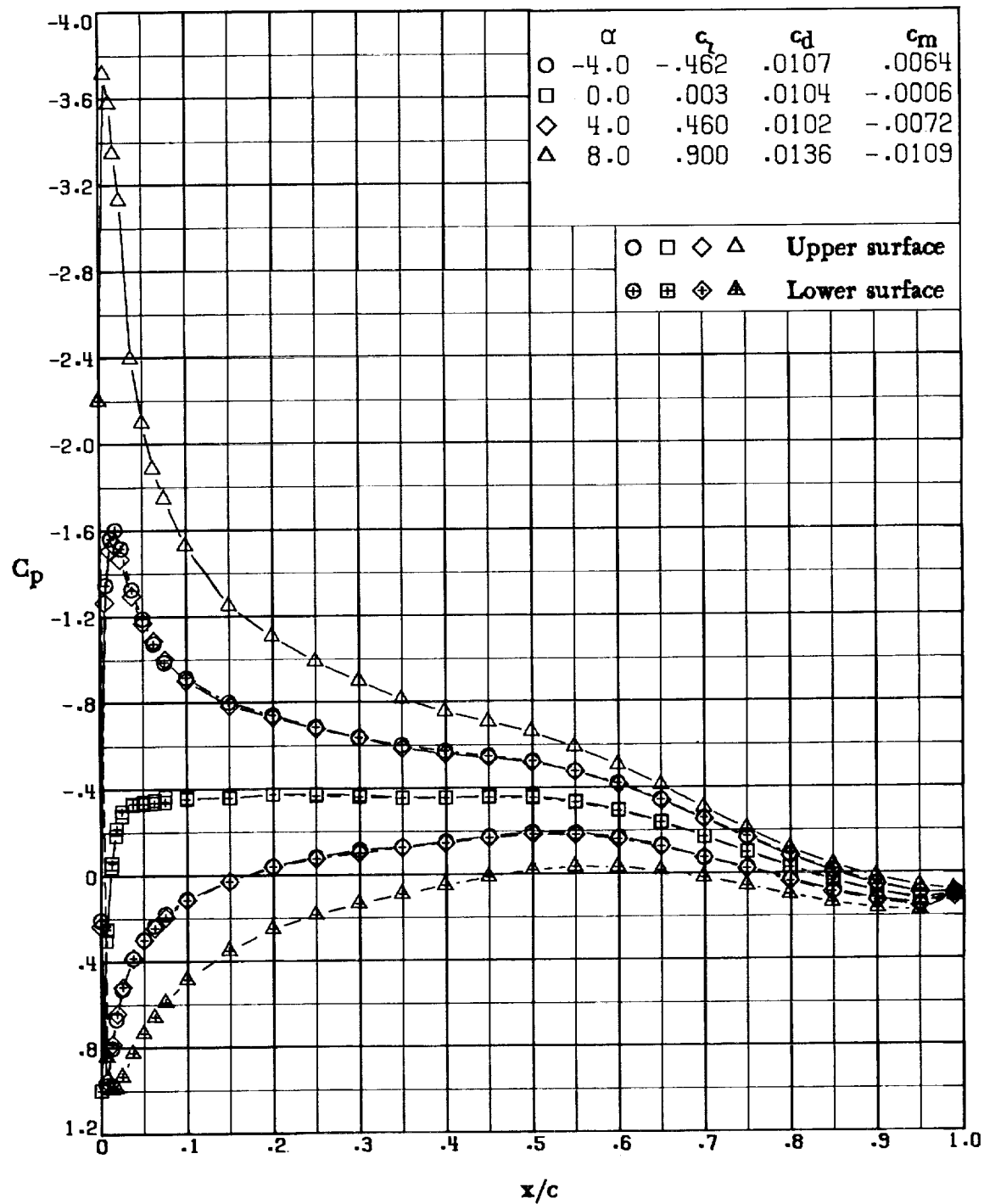
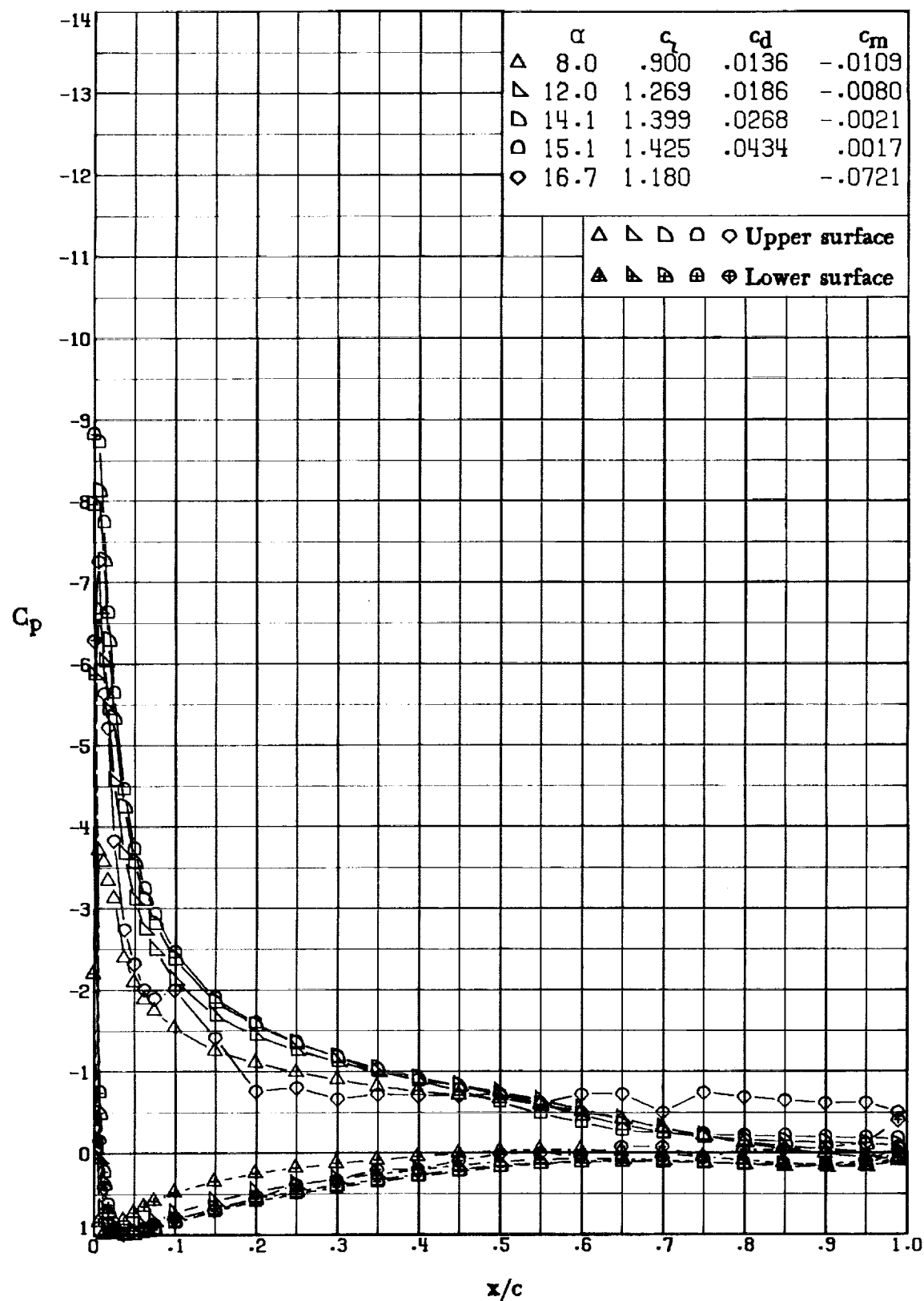


Figure 9. Effect of Mach number on section characteristics for NASA LS(1)-0013 airfoil at  $R = 6.0 \times 10^6$  with transition fixed at 0.075c.



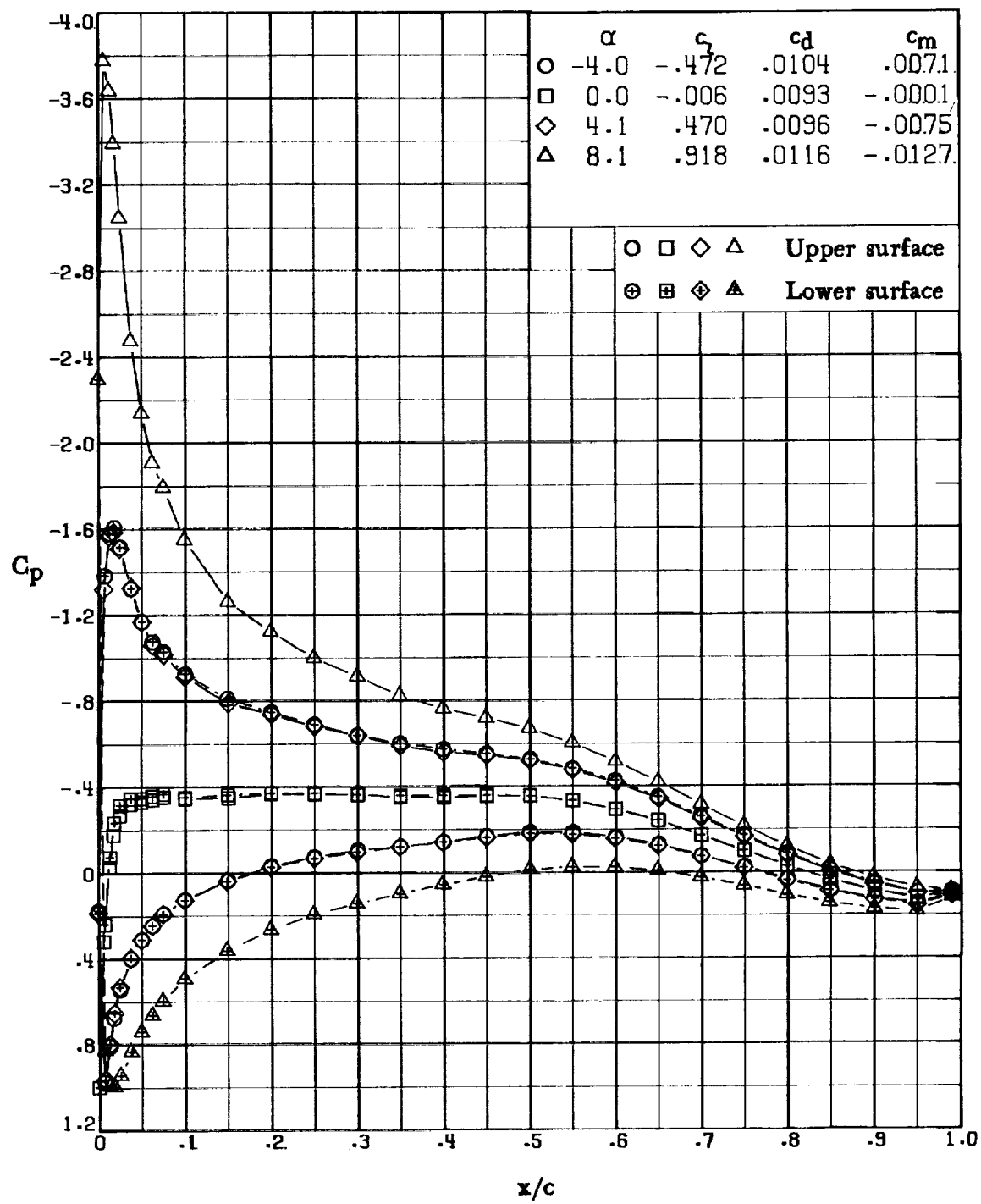
(a)  $\alpha \leq 8.0^\circ$ .

Figure 10. Effect of angle of attack on pressure distribution for NASA LS(1)-0013 airfoil at  $M = 0.15$  and  $R = 2.2 \times 10^6$  with transition fixed at  $0.075c$ .



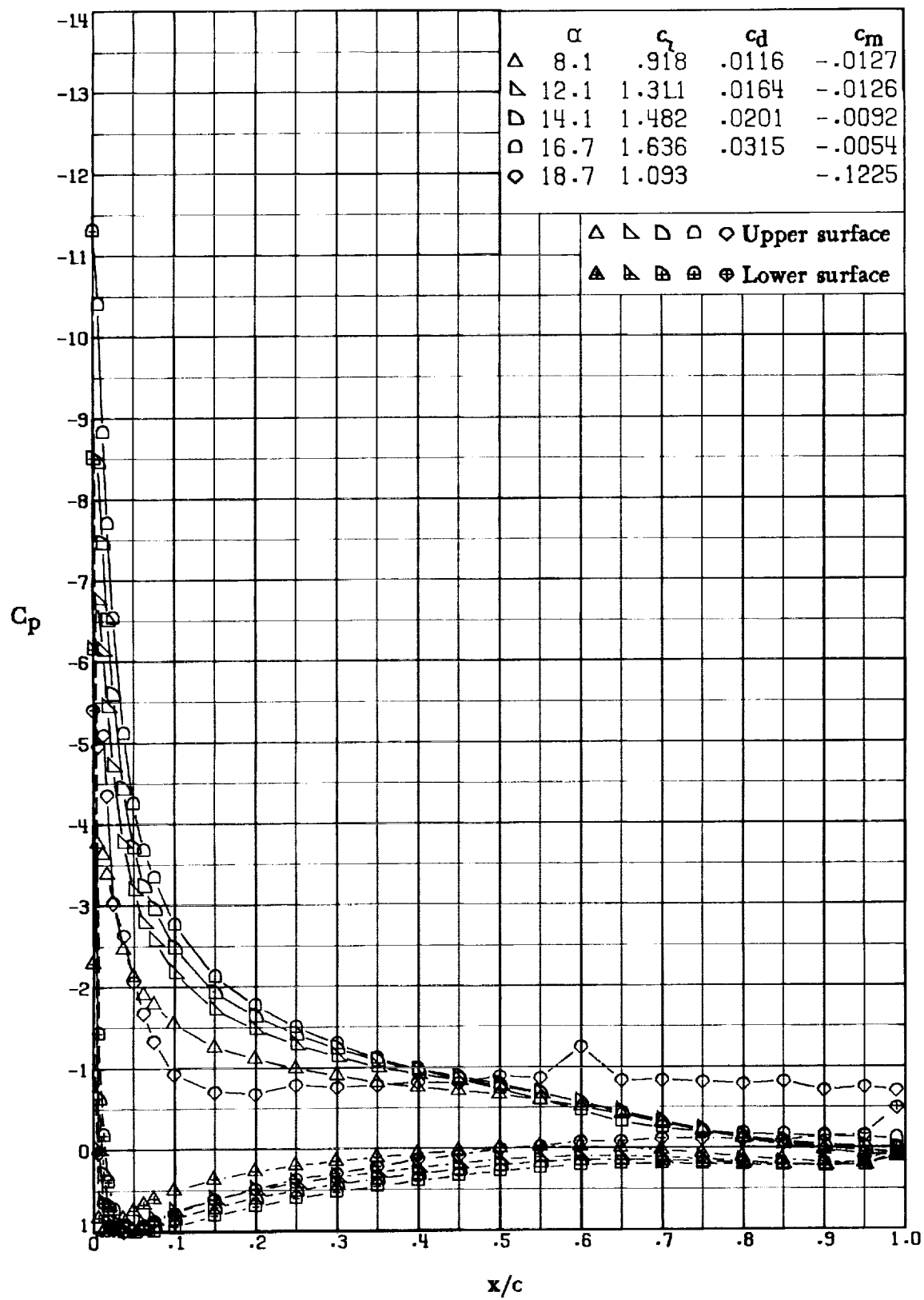
(b)  $\alpha \geq 8.0^\circ$ .

Figure 10. Concluded.



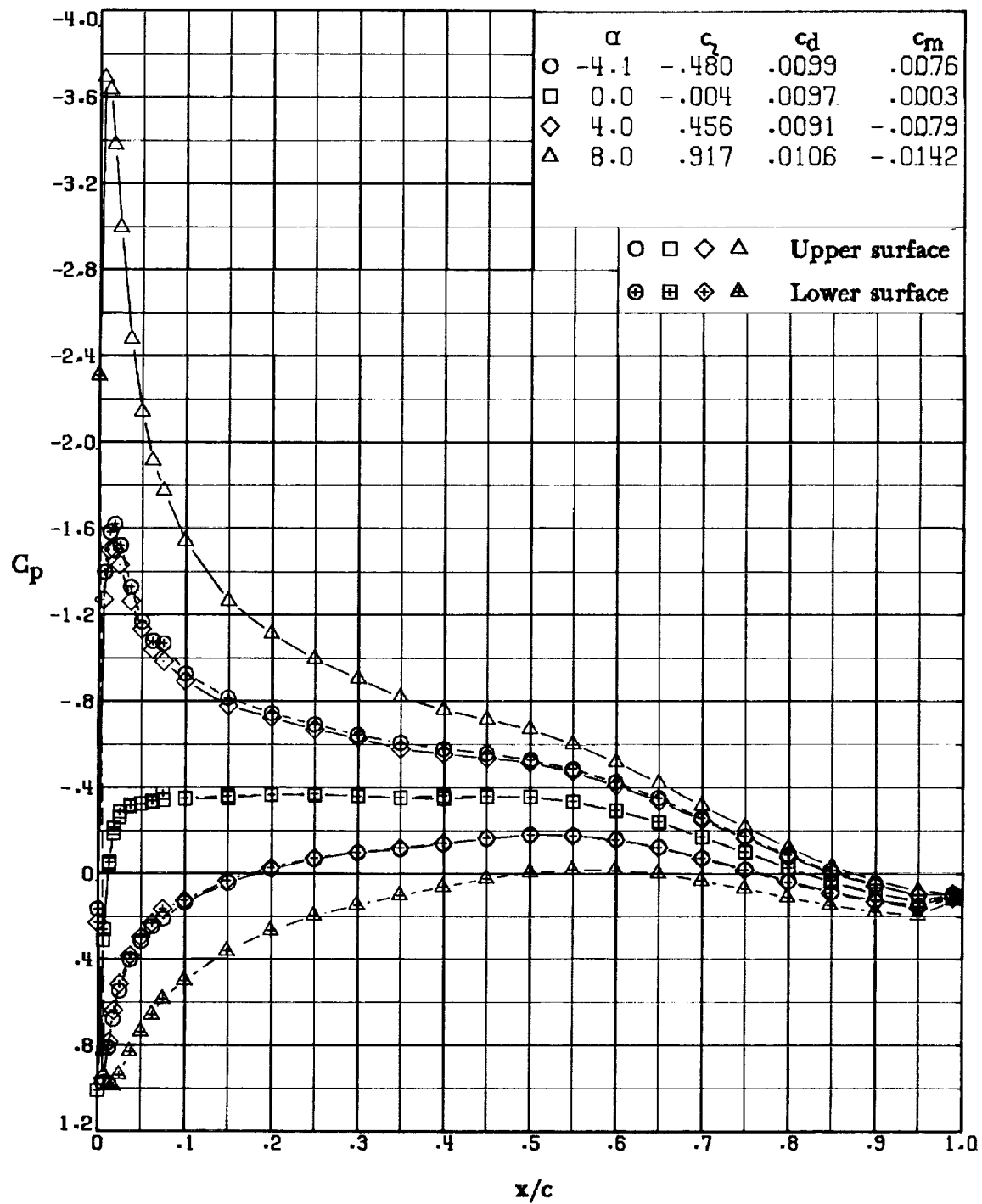
(a)  $\alpha \leq 8.1^\circ$ .

Figure 11. Effect of angle of attack on pressure distribution for NASA LS(1)-0013 airfoil at  $M = 0.15$  and  $R = 4.0 \times 10^6$  with transition fixed at 0.075c.



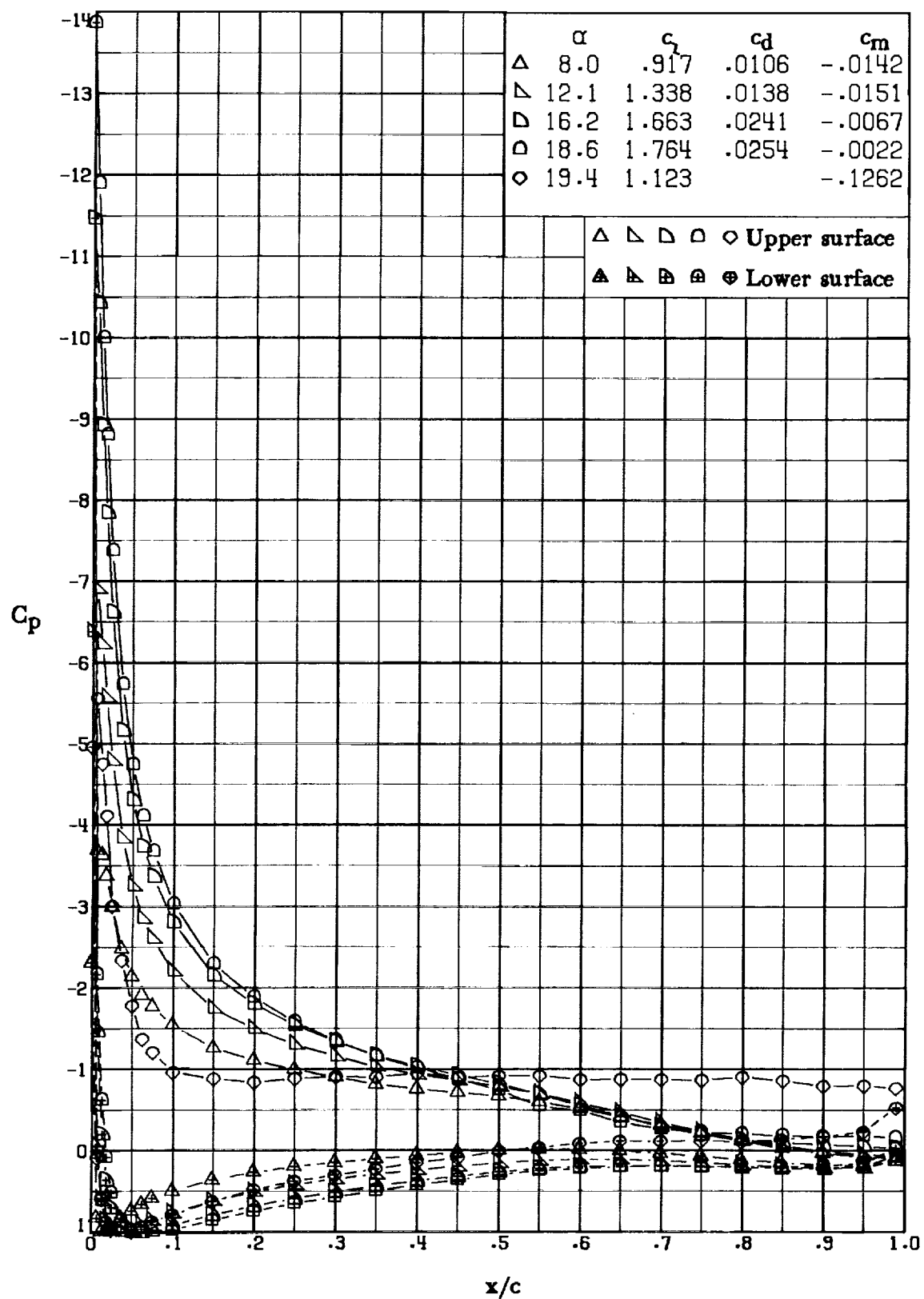
(b)  $\alpha \geq 8.1^\circ$ .

Figure 11. Concluded.



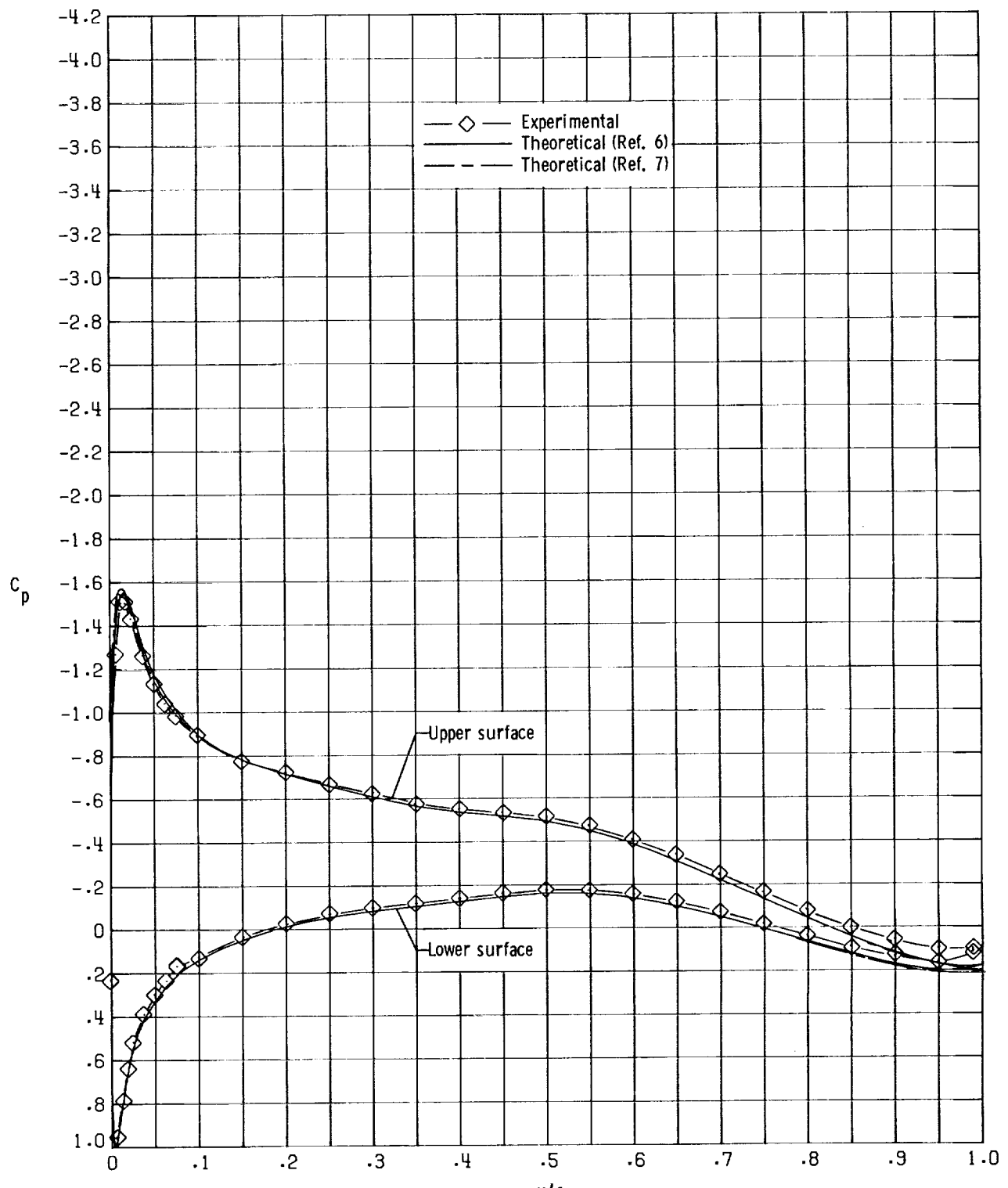
(a)  $\alpha \leq 8.0^\circ$ .

Figure 12. Effect of angle of attack on pressure distribution for NASA LS(1)-0013 airfoil at  $M = 0.15$  and  $R = 6.0 \times 10^6$  with transition fixed at  $0.075c$ .



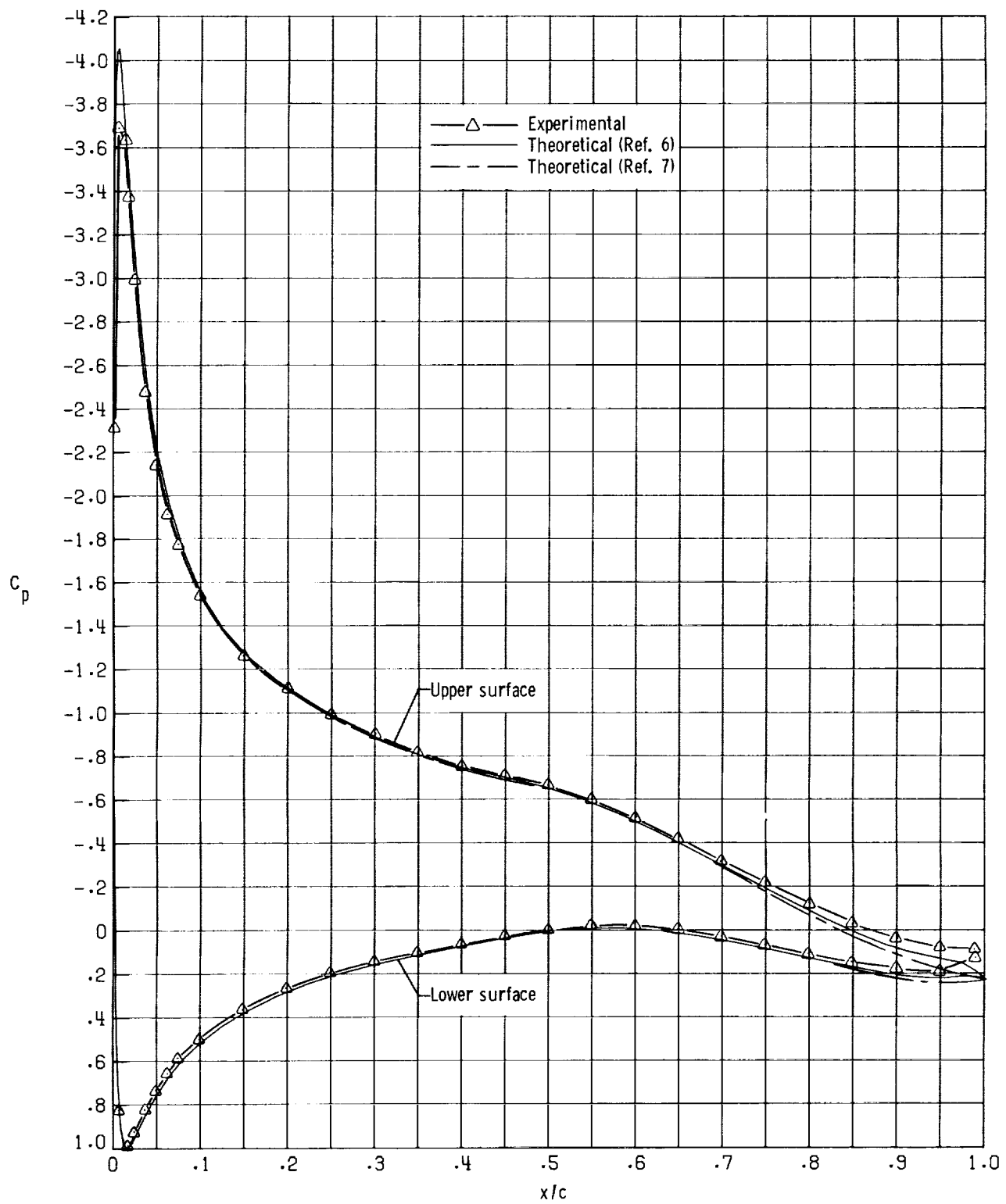
(b)  $\alpha \geq 8.0^\circ$ .

Figure 12. Concluded.



(a)  $\alpha = 4^\circ$ .

Figure 13. Comparison of experimental and theoretical chordwise pressure distributions for NASA LS(1)-0013 airfoil at  $M = 0.15$  and  $R = 6.0 \times 10^6$  with transition fixed at  $0.075c$ .



(b)  $\alpha = 8^\circ$ .

Figure 13. Concluded.

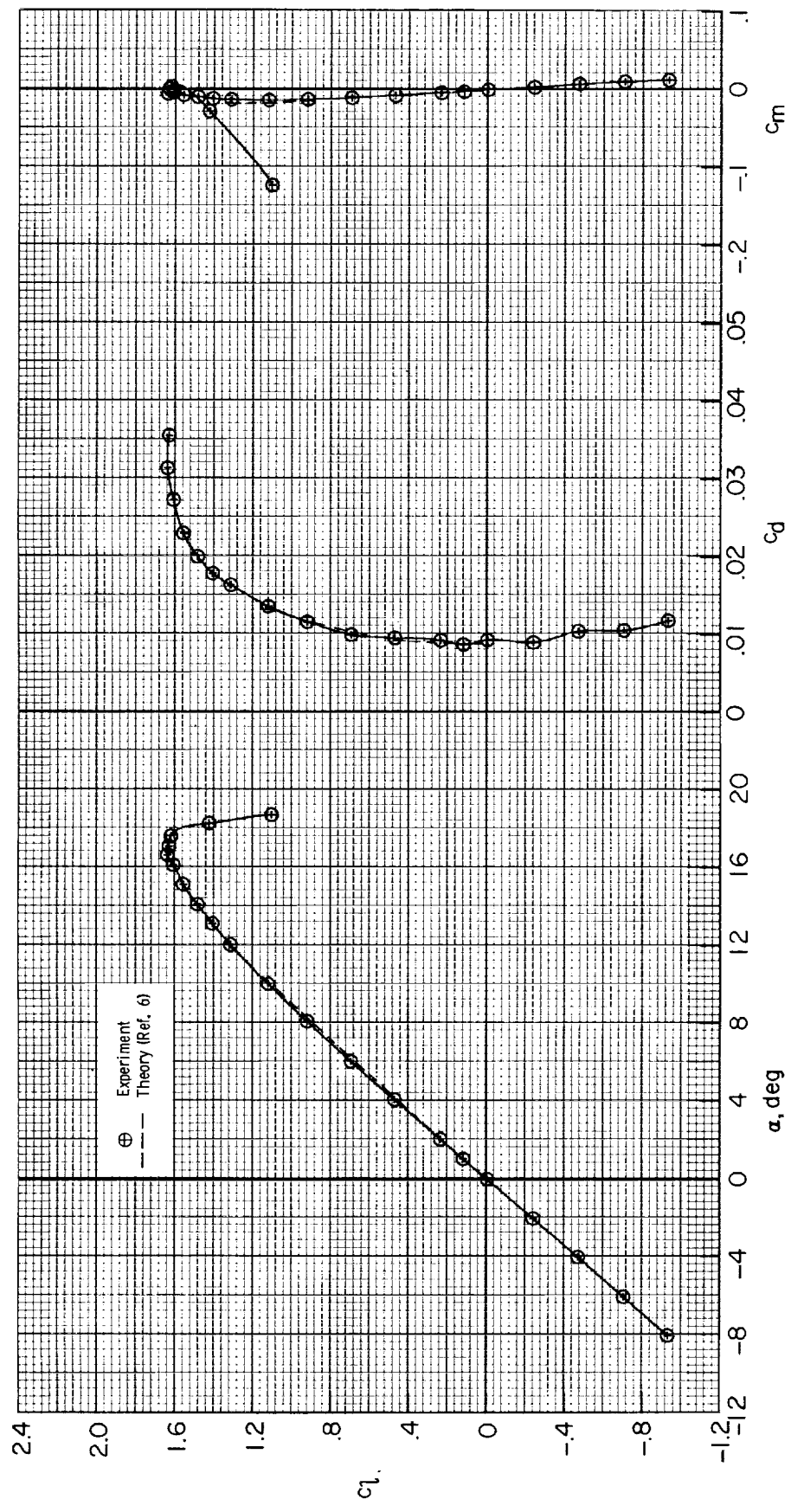


Figure 14. Comparison of experimental and theoretical section characteristics for NASA LS(1)-0013 airfoil at  $M = 0.15$  and  $R = 4.0 \times 10^6$  with transition fixed at  $0.075c$ .

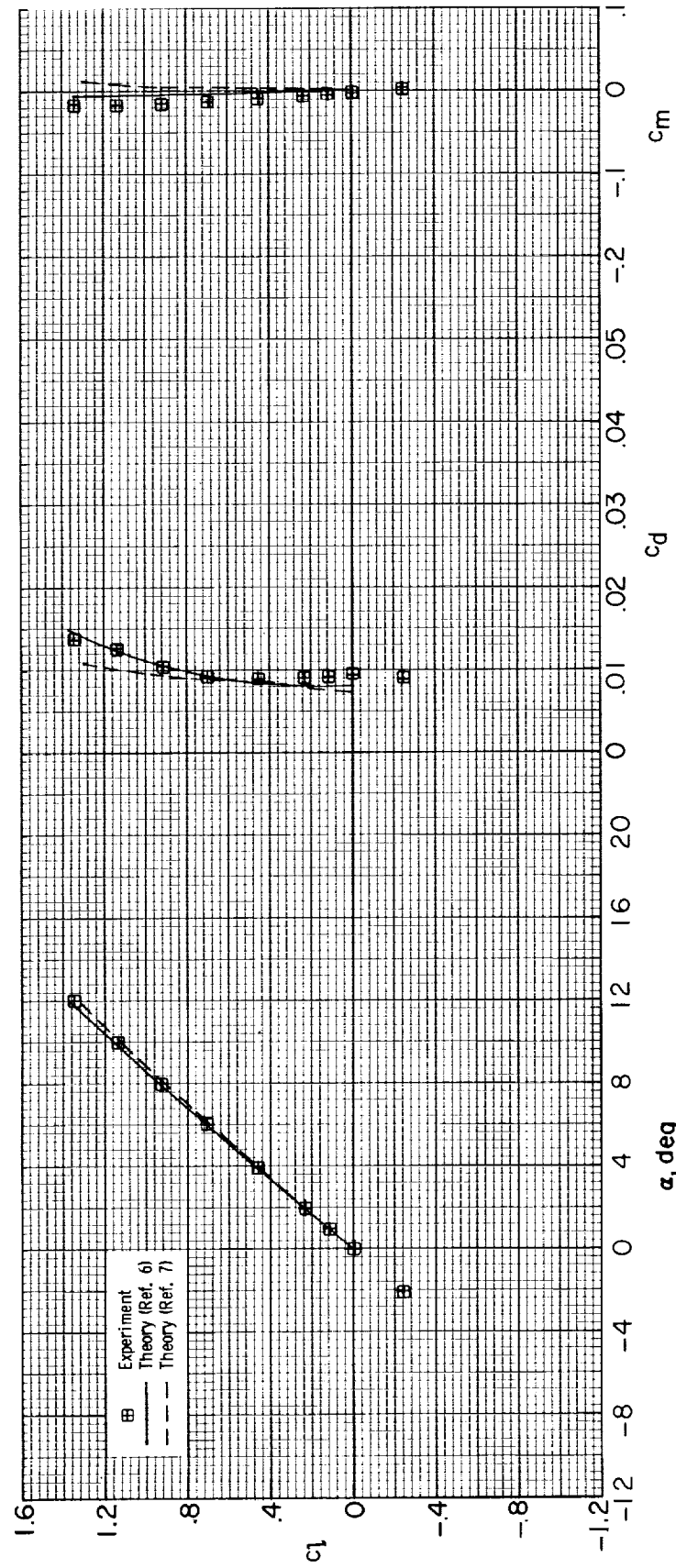
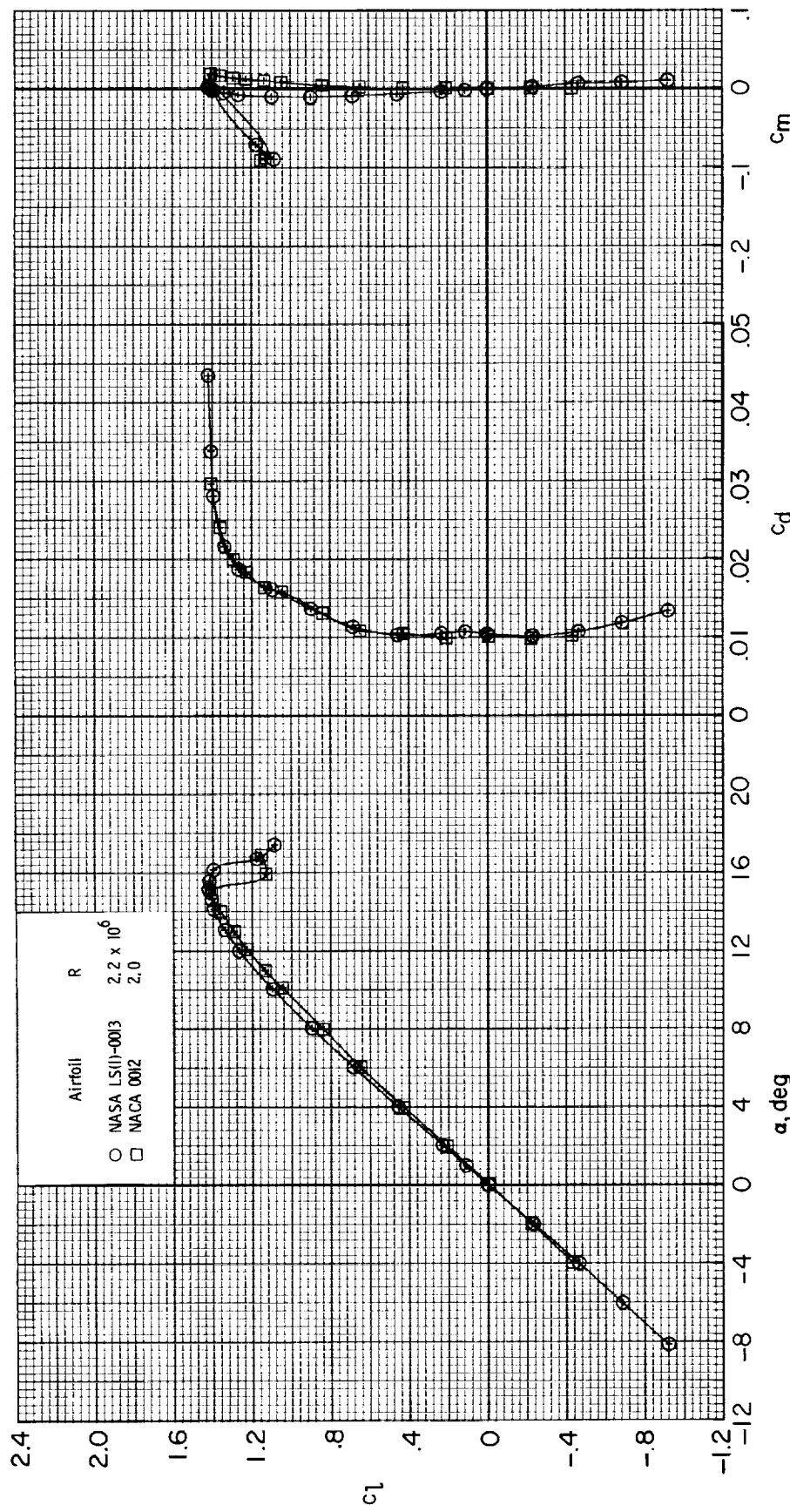
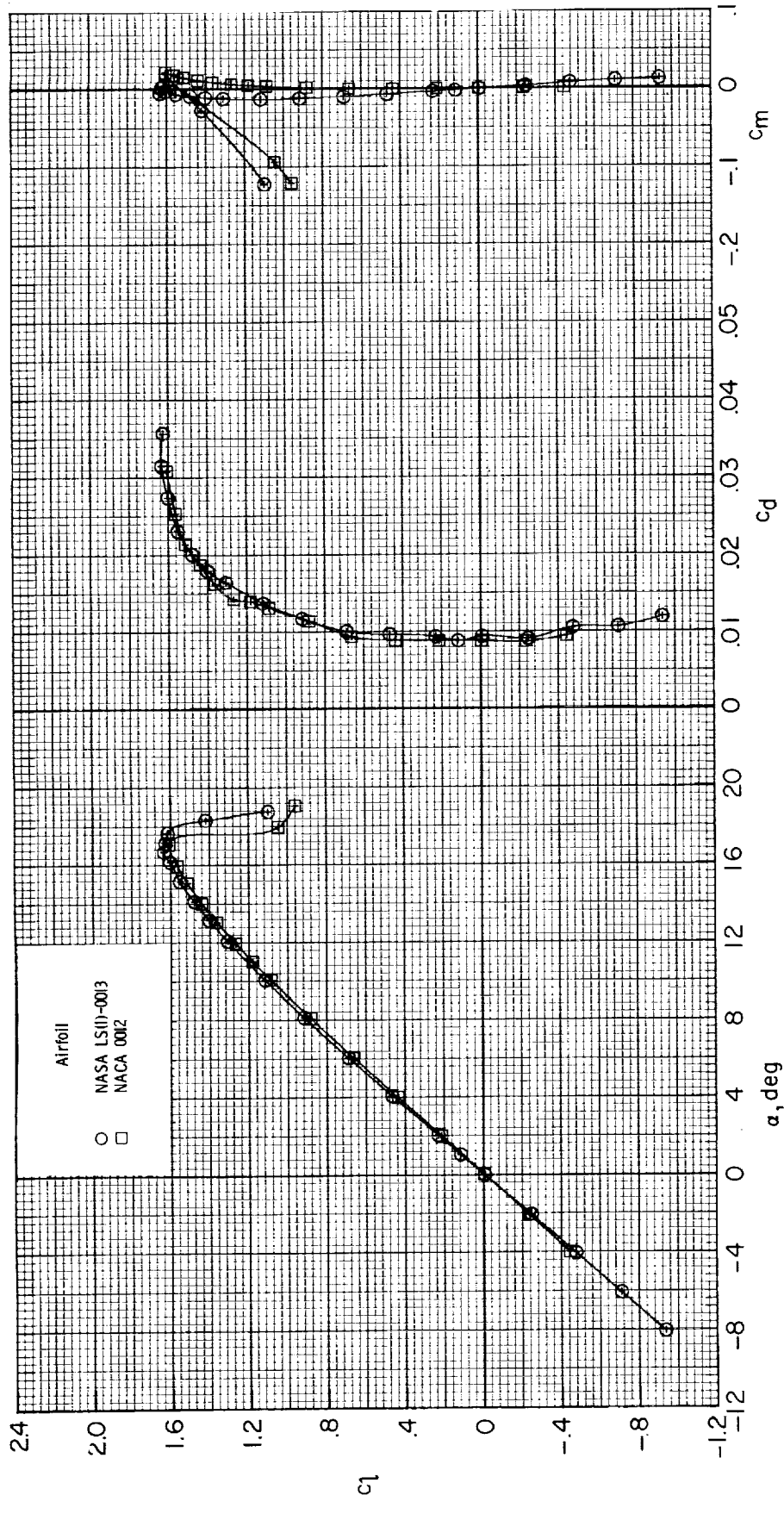


Figure 15. Comparison of experimental and theoretical section characteristics for NASA LS(1)-0013 airfoil at  $M = 0.15$  and  $R = 6.0 \times 10^6$  with transition fixed at  $0.075c$ .



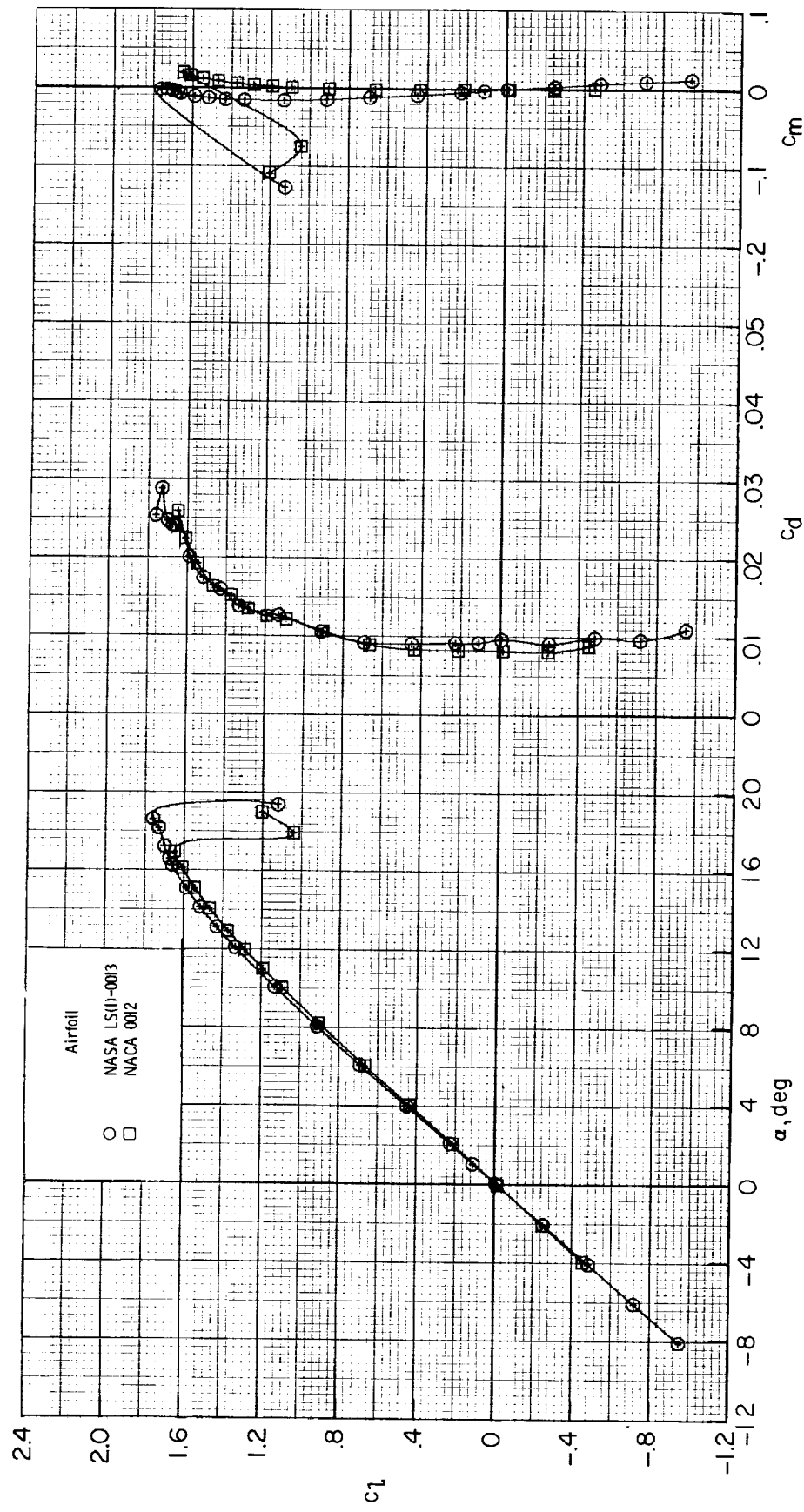
(a)  $R = 2.0 \times 10^6$ .

Figure 16. Comparison of section characteristics for NASA LS(1)-0013 and NACA 0012 airfoils at  $M = 0.15$  with transition fixed at 0.075c.



(b)  $R = 4.0 \times 10^6$ .

Figure 16. Continued.



(c)  $R = 6.0 \times 10^6$ .

Figure 16. Concluded.

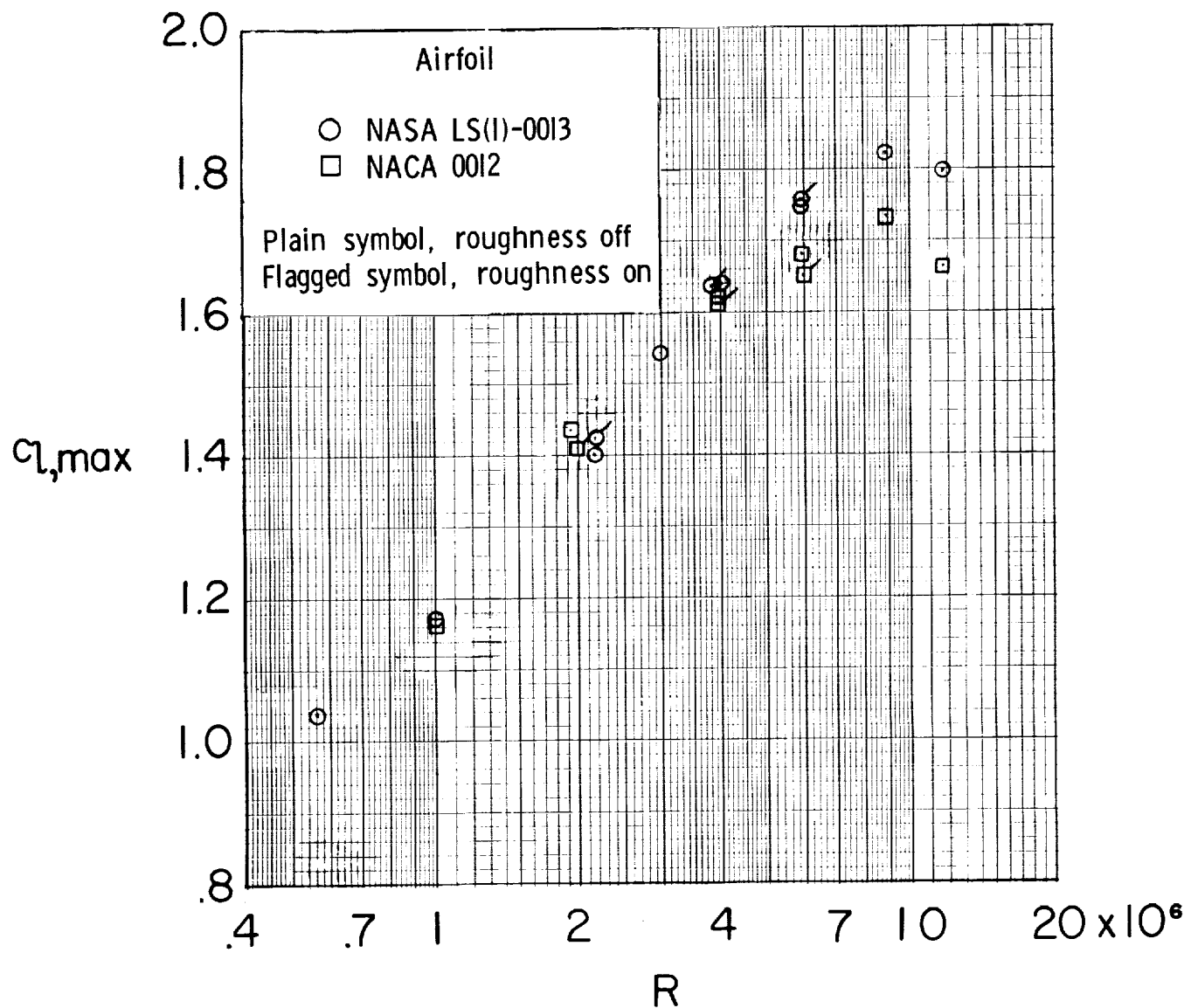


Figure 17. Variation of maximum section lift coefficient with Reynolds number for NASA LS(1)-0013 and NACA 0012 airfoils at  $M \leq 0.15$ .

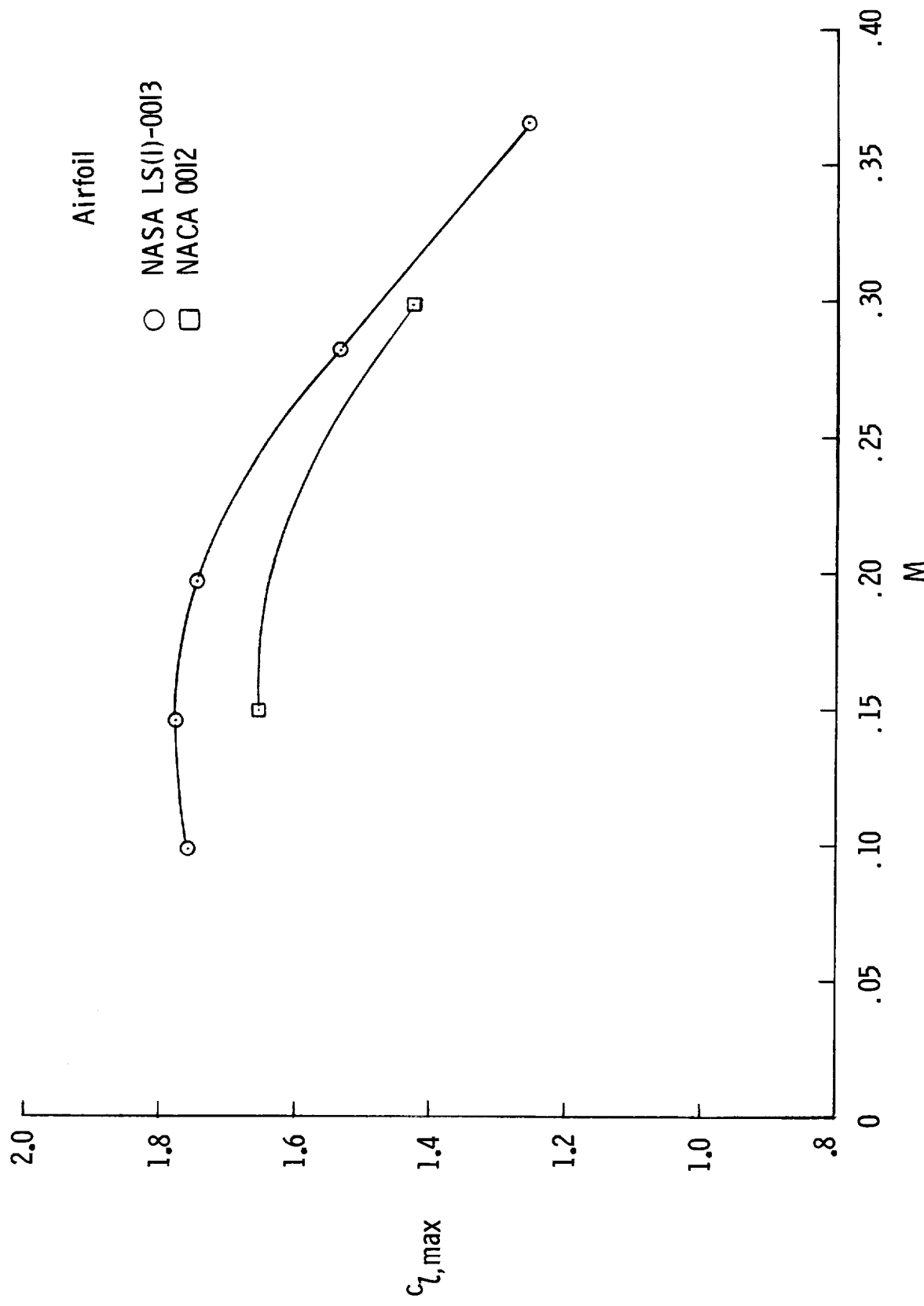


Figure 18. Variation of maximum section lift coefficient with Mach number for NASA LS(1)-0013 and NACA 0012 airfoils at  $R = 6.0 \times 10^6$  with transition fixed at  $0.075c$ .

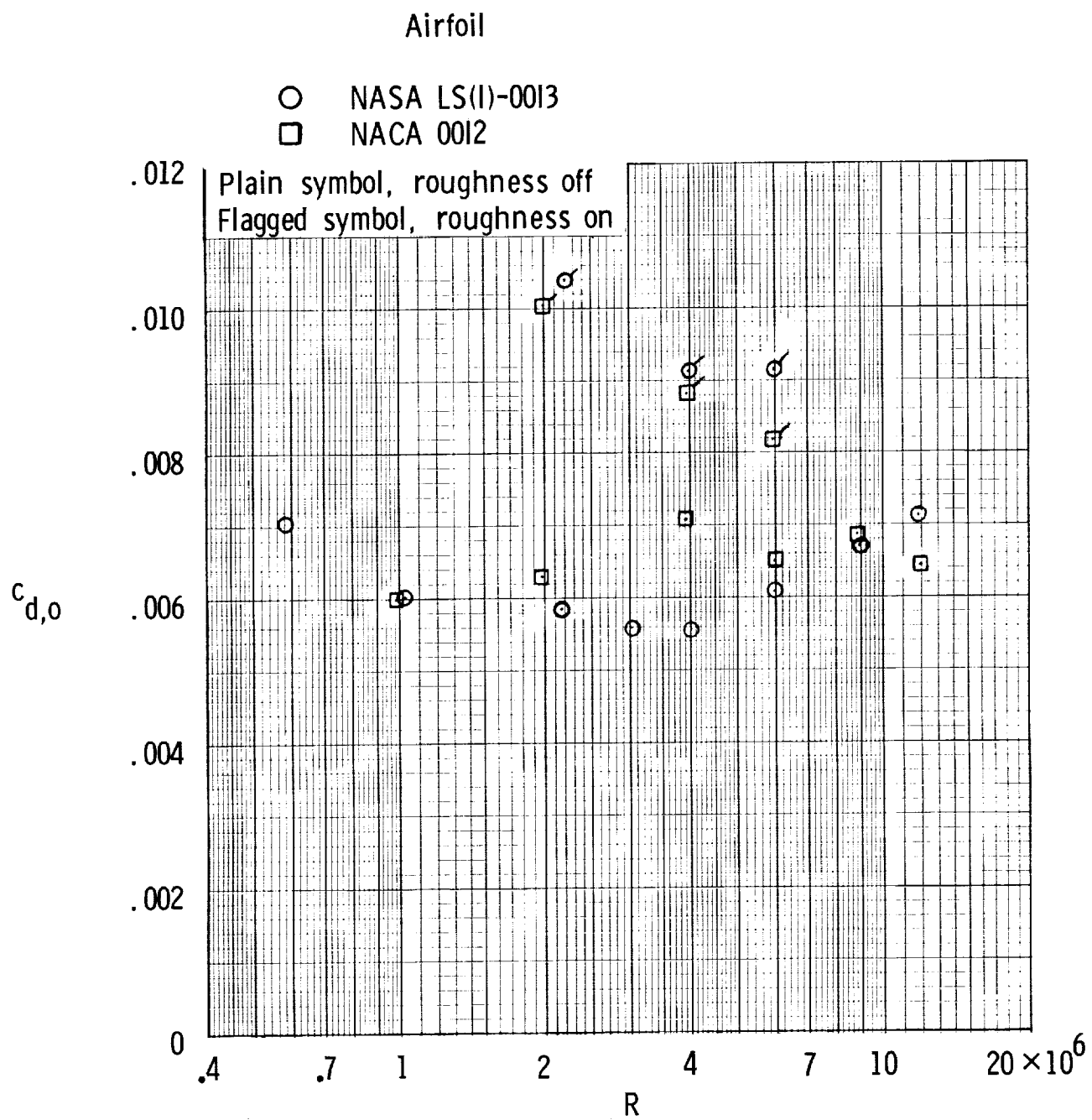


Figure 19. Variation of zero-lift drag coefficient with Reynolds number for NASA LS(1)-0013 and NACA 0012 airfoils at  $M \leq 0.15$ .

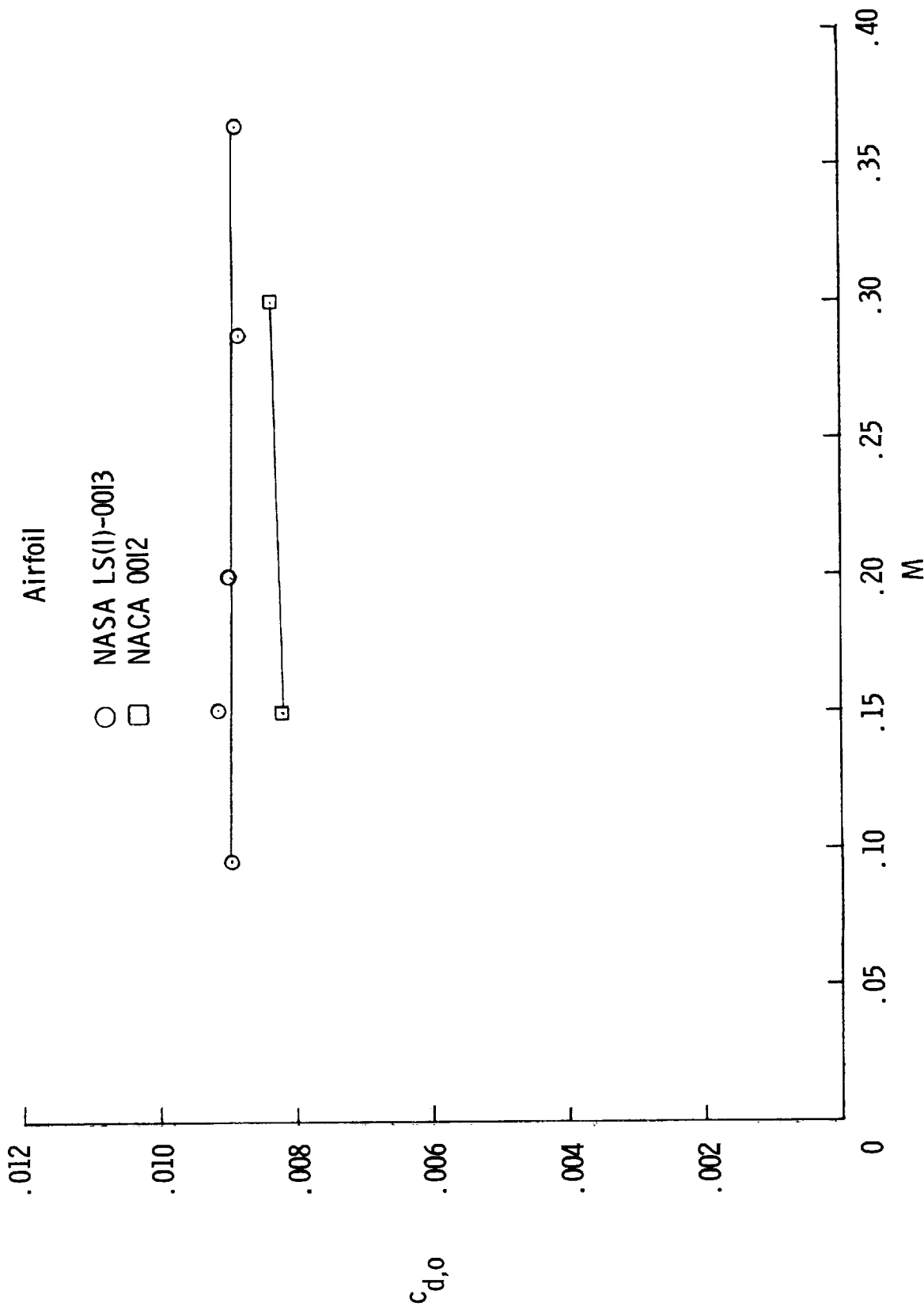
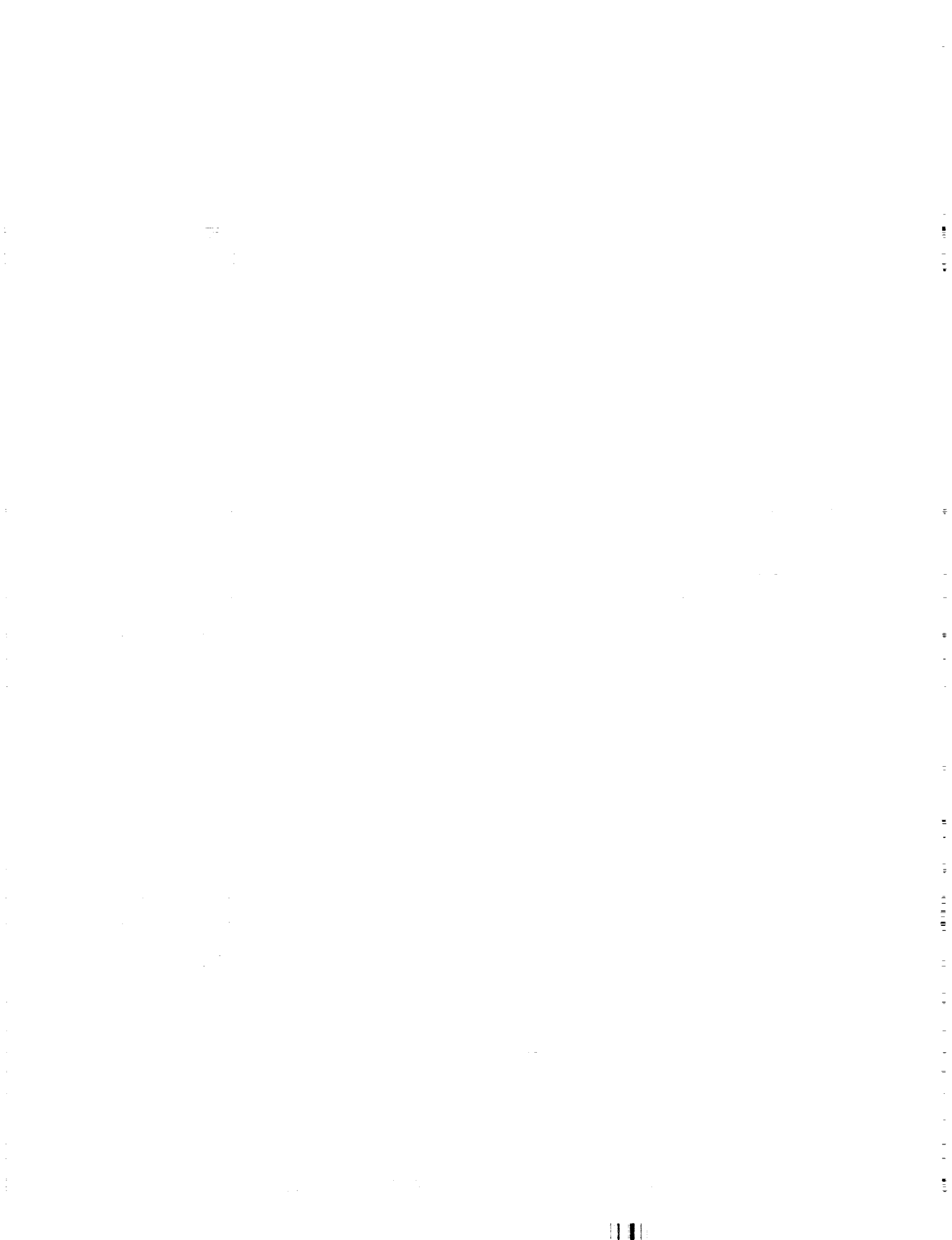


Figure 20. Variation of zero-lift drag coefficient with Mach number for NASA LS(1)-0013 and NACA 0012 airfoils at  $R = 6.0 \times 10^6$  with transition fixed at 0.075c.





## Report Documentation Page

1. Report No. NASA TM-4003	2. Government Accession No.	3. Recipient's Catalog No.	
4. Title and Subtitle Low-Speed Wind-Tunnel Results for Symmetrical NASA LS(1)-0013 Airfoil		5. Report Date August 1987	
		6. Performing Organization Code	
7. Author(s) James C. Ferris, Robert J. McGhee, and Richard W. Barnwell		8. Performing Organization Report No. L-16279	
9. Performing Organization Name and Address NASA Langley Research Center Hampton, VA 23665-5225		10. Work Unit No. 505-60-21-01	
		11. Contract or Grant No.	
12. Sponsoring Agency Name and Address National Aeronautics and Space Administration Washington, DC 20546-0001		13. Type of Report and Period Covered Technical Memorandum	
		14. Sponsoring Agency Code	
15. Supplementary Notes			
16. Abstract A wind-tunnel test has been conducted in the Langley Low-Turbulence Pressure Tunnel to evaluate the performance of a symmetrical NASA LS(1)-0013 airfoil which is a 13-percent-thick, low-speed airfoil. The airfoil contour was obtained from the thickness distribution of a 13-percent-thick, high-performance airfoil developed for general aviation airplanes. The tests were conducted at Mach numbers from 0.10 to 0.37 over a Reynolds number range from about $0.6 \times 10^6$ to $12.0 \times 10^6$ . The angle of attack varied from about $-8^\circ$ to $20^\circ$ . The results indicate that the aerodynamic characteristics of the present airfoil are similar to, but slightly better than, those of the NACA 0012 airfoil.			
17. Key Words (Suggested by Authors(s)) NASA LS(1)-0013 airfoil Experimental Theoretical Low speed Reynolds number variation Symmetrical		18. Distribution Statement Unclassified - Unlimited	
Subject Category 02			
19. Security Classif.(of this report) Unclassified	20. Security Classif.(of this page) Unclassified	21. No. of Pages 36	22. Price A03

